Heliyon 10 (2024) e35748

Contents lists available at ScienceDirect

Heliyon

journal homepage: www.cell.com/heliyon

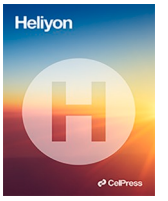

Research article

Enhancing thermodynamic performance with an advanced combined power and refrigeration cycle with dual LNG cold energy utilization

Tajwar A. Baigh , Mostofa J. Saif , Ashraf Mustakim , Fairooz Nanzeeba , Yasin Khan , M. Monjurul Ehsan *

Department of Mechanical and Production Engineering (MPE), Islamic University of Technology (IUT), Board Bazar, 1704, Gazipur, Bangladesh

A R T I C L E I N F O

Keywords:
Waste heat recovery
Multi-objective optimization
Exergy analysis
Cascade power cycle
Absorption refrigeration
Thermo-economic analysis

A B S T R A C T

Utilizing waste heat to drive thermodynamic systems is imperative for improving energy efficiency, thereby improving sustainability. A combined cooling and power systems (CCP) utilizes heat from a temperature source to deliver both power and cooling. However, CCP systems utilizing LNG cold energy suffers from low second law efficiency due to significant temperature differences. To address this, an "Advanced Power and Cooling with LNG Utilization (ACPLU)" system is proposed, integrating a cascaded transcritical carbon dioxide (TCO_2)-LNG cycle with an Organic Rankine cycle (ORC) for improved power generation and an absorption refrigeration system (ARS) for simultaneous cooling. This study evaluates the second law efficiency, net work output, and exergy destruction performance through a sensitivity analysis, optimizing variables such as heat source temperature, superheater temperature difference, ORC and CO_2 turbine inlet and condenser pressures, evaporator temperature, and pinch point temperatures of heat exchangers and generator. Compared to previous studies on CCP systems, the ACPLU shows a superior performance, with a second law efficiency of 27.3 % and a net work output of 11.76 MW. Cyclopentane as an ORC working fluid resulted in the highest second law efficiency of 29.06 % and net work output of 12.27 MW. Parametric analysis suggested that heat source temperature significantly impacts net power output. The exergy analysis concluded that a high-pressure ratio and good thermal match between the heat exchangers enhance overall performance. Utilizing artificial neural network (ANN) to produce a multiple-input-multiple-output (MIMO) objective function and performing multi-objective optimization (MOO) using genetic algorithm (GA), an improved second law efficiency and net power output by 28.11 % and 14.16 MW respectively, with pentane as the working fluid, is demonstrated. An average cost rate of 9.121 $/GJ was observed through a thermo-economic analysis. The ACPLU system is promising for medium temperature waste heat recovery, such as, pharmaceutical manufacturing plants.

* Corresponding author.
E-mail address: ehsan@iut-dhaka.edu (M.M. Ehsan).

https://doi.org/10.1016/j.heliyon.2024.e35748
Received 20 February 2024; Received in revised form 25 July 2024; Accepted 2 August 2024
Available online 3 August 2024

Nomenclature

Abbreviation	
ORC	Organic Rankine cycle
TCO_2	Transcritical carbon dioxide
LNG	Liquefied natural gas
ARS	Absorption refrigeration system
HPHE	High-pressure heat exchanger
LPHE	Low-pressure heat exchanger
ARSHE	ARS heat exchanger
SHX	Solution heat exchanger
EV1, EV2	Expansion valve/throttling valves
CRF	Capital recovery factor
CEPCI	Chemical Engineering Plant Cost Index
Symbols	
T	Temperature [°C]
P	Pressure [bar]
h	Enthalpy [kJ kg^{-1}]
s	Entropy [kJ kg^{-1}]
$\dot{Q}_{component}$	Heat transfer rate of a system component [kW]
$\dot{W}_{component}$	Work done by a component in the system [kW]
$\dot{W}_{net}$	Net work done [kW]
$e_{state\ point}$	Specific exergy at state point: *1,2 … n* [kJ kg^{-1}]
$\dot{E}_{state\ point}$	Rate of exergy at state point *1,2 ….n* [kW]
$\dot{E}^{D}_{component}$	Exergy destruction [kW]
η	Isentropic efficiency [%]
ψ	Second law efficiency [%]
Δ	Difference
ξ	Effectiveness of ARS heat exchanger
$U_{component}$	Heat transfer coefficient of a system component [kW/m^2.K]
$A_{component}$	Area of heat transfer of a system component [m^2]
$Z_{component}$	Capital cost of a system component [$]
$\dot{Z}_{component}$	Capital cost rate of a system component [$/h]
i_r	Interest rate
n	Time of operation [years]
γ	Operation and maintenance factor
τ	Annual operation time of the system system [h]
c_{system}	Average cost per unit energy [$/GJ]
Subscripts	
1, 2, 3,4 ….	State points
in	Inlet
out	Outlet
0	Dead state
VG	Vapor generator
sup	Superheater
gen	Generator
cond	Condenser
evp	Evaporator
abs	Absorber
tur	Turbine
CF	Counter-flow
PF	Parallel-flow
w	Water
wof	Working fluid
ph	Physical exergy
ch	Chemical exergy
ki	Kinetic exergy
po	Potential exergy
s	isentropic

1. Introduction

Thermal energy loss, or waste heat, is a major issue in industries, especially those which involves complex systems made up of a large number of components [1]. Approximately 60 % of the waste heat produced by these systems is reportedly emitted back into the atmosphere [2], contributing significantly to global warming. Therefore, waste heat recovery (WHR) is seen as one potential solution for enhancing system efficiency and reducing its environmental impact [3]. WHR systems utilizes the high temperature of exhaust gases of primary systems to produce useful work [4]. The most common heat sources for waste heat are internal combustion engines, gas turbines, diesel engines and industrial processes such as cement-production [5]. Developing a good WHR system, works in tandem with developing a more efficient thermodynamic system with a strong emphasis on sustainability.

1.1. Organic Rankine cycle (ORC)

Over the past 20 years, the market for Organic Rankine Cycle (ORC) plants has experienced a remarkable expansion, especially in developing WHR systems. By the end of 2016, there were about 563 powerplants with ORCs installed, generating an additional power of 2.75 GWe [6]. Due to its capacity for heat recovery from a wide range of temperatures (especially low heat), compactness, simple structure, high efficiency, low pollution, and minimal erosion, the ORC's development came with numerous potential application [2,4]. Low-temperature waste heat recovery from solar [6], geothermal [7] etc. have been used in ORC systems to produce energy. ORC systems can also be connected to various energy systems like power plants [8], biogas plants [9], energy storage systems [10] and even absorption refrigeration systems [11] because of its adaptability and reliable operation. Numerous studies have also found links between the ORC and high- and moderate-temperature heat sources (450 °C and above) [12]. The configuration of ORC plants can also be altered, and a variety of working fluids can be used in them. To enhance power output and achieve high efficiency, both factors must be optimized [13]. Due to the already-low operating temperatures of the ORC, cascading it with different cycles proves to be challenging, and only a handful of working fluids such as carbon dioxide (CO_2) [4] or liquid nitrogen [2] are suitable.

1.2. Transcritical CO_2 cycle (TCO_2) and LNG cold utilization

The high performance of a supercritical or transcritical CO_2 cycle, especially on electricity generation from a low-temperature heat source are recognized [14]. Furthermore, CO_2 is easy to obtain, non-toxic, non-flammable, non-explosive, and does not produce any detrimental environmental effects when utilized in a cycle [14,15]. However, the condensation of CO_2 is a significant issue in practice due to its low critical temperature. For low-temperature heat sources (specifically below 400 °C), ORC proves to be superior to CO_2-cycles when water is available as a cooling medium [13]. However, if a working fluid with a lower operating temperature than water is used in the heat sink, CO_2 power cycles would offer a relatively better performance for low-temperature heat recovery. To that end, a low temperature heat sink medium such as liquified natural gas (LNG) offers itself as a potential option.

LNG, in its liquid form, possesses a substantial amount of utilizable cold energy. The cold energy in one tonne of LNG can produce roughly 240 kWh of electricity, if fully utilized [16]. Re-gasification is also required before LNG can be used for its conventional use in heating or cooking. Typically, sea water is used to heat up the cold LNG liquid. However, in addition to energy consumption to run the sea water pump, the process may also harm the marine habitat. Hence, this process leads to substantial amounts of the cold exergy in the liquified LNG being wasted [17]. LNG has both thermal and mechanical energy. The expansion process is the only technique employed to utilize its mechanical exergy. The thermal side, however, offers additional choices, especially as a heat sink. Designing a power plant with nearly no emissions can also help with CO_2 capture [18].

It is generally known that the exergy efficiency of a heat exchanger suffers because of the substantial difference in the average temperatures between the hot and cold streams [5]. This issue arises because the LNG cycle operates at a relatively lower temperature than most working fluid's condensation temperature. To address this, many waste heat recovery systems utilizing low-temperature heat sources such as geothermal energy [19], solar energy [20] etc have been proposed that use a TCO_2 cycle with an LNG stream heat sink. However, such single-stage cycles still shared the common problem of having a large difference in temperature between the hot and cold side of the heat exchanger that was coupled with the LNG stream [21]. Hence, it can be concluded that, the usage of LNG as a heat sink for an efficient power cycle like a TCO_2 cycle should be combined with a cycle that allows the CO_2 to operate in the transcritical region, while also providing a facile development of power and LNG gas without having a significant difference in operating temperatures, i.e an ORC. LNG for a combined cycle, such as ORC and TCO_2 [22], shows great promise in providing effective waste heat utilization from a medium temperature heat source of 250 °C.

1.3. Features of absorption refrigeration system (ARS)

An ongoing field of study in refrigeration focuses on developing systems that does not wholly depend on electricity to regulate pressure such as the extensively studied vapor compression refrigeration (VCR) system [23–25]. An absorption refrigeration system (ARS) is a potential solution as it is a type of cooling appliance that draws its cooling power from an external heat source, such as waste heat [26], solar [27], geothermal [28], and biomass [29] in addition to electricity, making it a thermally active system. By absorbing a fluid vapor (e.g., ammonia, lithium bromide) into another carrier liquid (e.g., water), then pumping this solution to a high-pressure cycle with a basic pump and, finally producing vapours of the mixed solution by absorbing heat from the environment, produces the desired refrigeration effect. The development of ARS is mainly focused towards improving its refrigeration effect [11,30,31]. One way to improve the refrigeration effect is the integrating of the ARS with a traditional VCR system [32,33]. Different modifications of the ARS can also have an effect in its performance. For example, changing a double-effect ARS from a series to parallel arrangement can improve the coefficient of performance (COP) from 1.39 to 1.44 [34].

ARS technology has shown great potential in using waste heat as its energy source. An ARS system integrated with a bulk carrier engine to recover heat and produce refrigeration can, theoretically, reduce electricity consumed for air-conditioning by about 70 % and 61 % in ISO and tropical conditions respectively. This is estimated to save about 95 tonnes of fuel annually [35]. Furthermore, the integration of ARS utilizing waste heat to an existing plant, such as an LNG producing plant for sub-cooling of the LNG, can lead to a COP improvement of about 63 % [36]. Experimental evaluation of ARS utilizing exhaust heat have shown satisfactory performance in between the temperature range of 150 °C–350 °C [37]. In conclusion, ARS technology is dependable, reasonably priced, and has great prospects as a sustainable refrigeration system. However, due to stand-alone ARS's providing inadequate cooling for high-level industrial use, the adoption of the ARS is still not feasible. Thereby, in order to improve the feasibility of the ARS, combing them with

power-producing systems to make a combined cooling and power system (CCP) is a potential solution.

1.4. Combined cooling and power systems (CCPs)

A combined cooling, heating, and power (CCHP) system has many advantages compared to a conventional stand-alone system, such as: higher efficiency and power, along with reduced emission of CO_2 gas [38,39]. A simpler derivation of the CCHP is the combined cooling and power (CCP) system, which have been extensively used for developing WHR systems.

For performance evaluation of a WHR system, one of the crucial assessment areas is the reduction of the waste heat outlet temperature, i.e., more effective utilization of the heat possessed by the waste stream before being exhausted out. To achieve that, recent studies have focused on the effect of integrating an ARS into power cycles, such as: combining supercritical CO_2 with ORC or recompression Brayton cycle, or both [40,41]; TCO_2 cycles [42], and ORCs with CO_2 capturing storage (CCS) [43]. The combination of ARS and LNG subsystems for enhanced cooling was also explored [44]. CCP systems such as a Kalina cycle integrated with an ARS improved the COP from 0.256 to 0.360, and the second law efficiency from 18.5 % to 46.8 %, in addition to producing 493 kW of power [45]. The integration of supercritical CO_2 (sCO_2) cycle with ARS studied by Li et al. [46], also reported an improvement in COP. The prior references elucidate the immense potential of integrating an ARS with CCPs. However, a research gap is presented on the usage of ARS systems with efficient cascaded systems such as ORC-TCO_2 systems with LNG energy utilization.

1.5. Problem statement and research scope

In this paper, an augmented combined cooling and power (CCP) waste heat recovery system is proposed. To better match the LNG cycle's low temperature, a transcritical carbon dioxide (TCO_2) cycle is used. However, as the average temperature between the heat source and the operable temperature range of the TCO_2 cycle is large, using the TCO_2 cycle for power generation severely limits effective heat energy utilization, especially for moderate to high temperature heat sources. Consequently, the second law efficiency suffers significantly. This novel "Advanced cooling and power with LNG utilization (ACPLU)" system addresses this concern by making use of an ORC, that has been reported by previous studies to have a good thermal match with waste heat in between the medium to high temperature range, as the top cycle. To enhance the utilization of the waste heat and the applicability of the ACPLU, an absorption refrigeration system (ARS) is integrated into the combined system to provide refrigeration, while using the LNG cycle as its condenser. This dual functionality of the LNG cold energy can increase the temperature of the LNG working fluid, which can then be used to rotate a turbine to produce additional useful work output. The LNG can also be assumed to be re-gasified by this time and can be redistributed to systems that uses gaseous LNG, such as chemical plants for manufacturing paint, or fertilizers and even medicine. A comparative analysis of different working fluids in the ORC of the ACPLU will be performed to identify which working fluid provides the best performance. To study whether the issue about the high exergy destruction is mitigated by the ACPLU, second law efficiency and net work output, as well as on the exergy destruction performance will be assessed through a sensitivity analysis. Finally, a multi-objective optimization (MOO) using artificial neural network (ANN) and genetic algorithm (GA) will be conducted to find the optimum combination of parameters. A pharmaceutical manufacturing plant boiler usually exhausts heat at a moderate temperature (at about 260 °C). The ACPLU is expected to utilize this exhaust heat to produce enough refrigeration to be utilized to store blood samples, vaccines, and medical drugs, while also generating power. Additionally, the re-gasified LNG can be used for in-house heating and cooking.

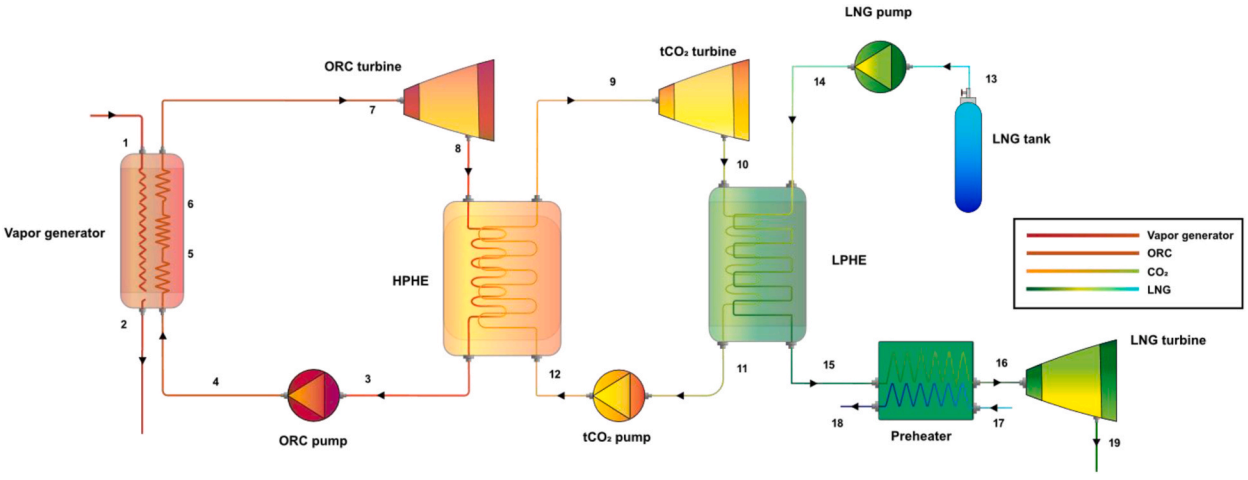

Fig. 1. Schematic of the ORC-TCO_2-LNG power cycle.

2. System description

2.1. Cascaded power cycle with LNG cold energy utilization

The heat source is assumed to be the moderate temperature exhaust gases at around 300 °C [5]. An illustration of the cascaded power system is depicted in Fig. 1. A vapor generator absorbs heat from the exhaust stream through an economizer, a heat exchanger, and an evaporator. The vapor generator exchanges heat with the ORC working fluid (top cycle). The superheated working fluid then expands in the turbine to generate power (state 7 to 8). Subsequently, it passes through the high-pressure heat exchanger, HPHE, condensing into a saturated liquid phase for the top cycle (from state 3 to 4). The bottom cycle consists of the transcritical CO_2 (TCO_2) cycle absorbs heat from the HPHE, effectively turning into supercritical vapor (state 9). After generating power by expansion by the turbine (state 10), the working fluid goes through the low-pressure heat exchanger (LPHE). An LNG open cycle is pumped into the LPHE from ambient pressure (1.01 bar) to 70 bar at −162 °C (state 13 to 14). The LNG is responsible for absorbing the heat from the LPHE (state 10 to 11) while also heating up the LNG stream (state 14 to 15). To utilize the cold energy further, a chiller is added in the LNG stream to produce cold water (state 15 to 16). This dual-effect cold energy utilization of the LNG increases working fluid temperature. Finally, this vaporized LNG is forced through a turbine and generates extra power before being sent out in its re-gasified form for further use.

2.2. Absorption refrigeration system (ARS)

Fig. 2 shows an illustration of a single-effect ARS. The generator is supplied with heat, which consists of a binary mixture of a fluid (LiBr) with water, water being the refrigerant. By absorbing heat, the lower boiling temperature fluid, i.e., water, vaporizes. The fluid is then condensed by expelling heat to the surrounding (state 2). The throttling valve (EV-1) expands the working fluid, which is then

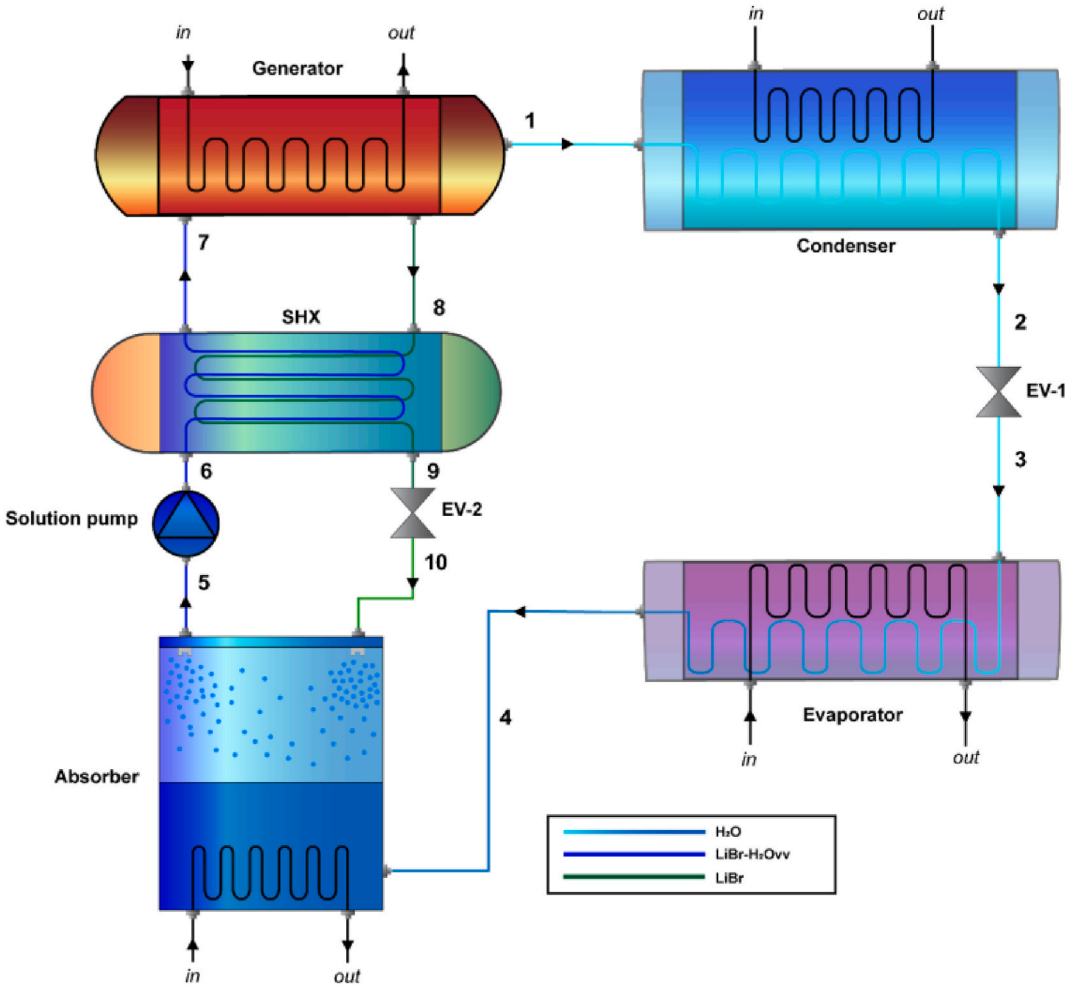

Fig. 2. Single-effect absorption refrigeration system.

transferred into the evaporator (state 3). The throttling process is characterized by the pressure reduction of the working fluid, which also reduces its temperature. The heat from the surrounding is absorbed by the evaporator's low-temperature fluid, resulting in the desired cooling. In the absorber, the concentrated LiBr solution absorbs the refrigerant (at state 4). This absorption process causes a reduction in evaporator pressure, resulting in the temperature of the fluid to reduce further. Hence, even after the heat is absorbed by the surrounding, the low temperature of the cold fluid can be maintained. When the solution cannot continue this absorption process, the once-again-binary solution is pumped back into the generator. A significant exergy destruction can occur after the binary solution is pumped into the generator again (state 7) as the generator needs to heat the binary fluid again to evaporate out the water and start the absorption process again. Hence, a solution heat exchanger, SHX, is used (state 6 to 7) which can preheat the binary solution by transferring heat from the concentrated LiBr solution (state 8 to 9) before it enters the generator. An additional throttling valve (EV-2) is used to cool the concentrated LiBr solution after it transfer heat to the binary solution (state 9 to 10).

2.3. Proposed ACPLU system

The schematic diagram shown in Fig. 3 shows the proposed CCP system. The ACPLU system combines a cascaded power cycle consisting of a vapor generator, three turbines, three pumps, two heat exchangers, and a preheater with a single-effect ARS that consists of a generator, a condenser (ARSHE), an evaporator and absorber, one heat exchanger (SHX), a pump, and two throttling

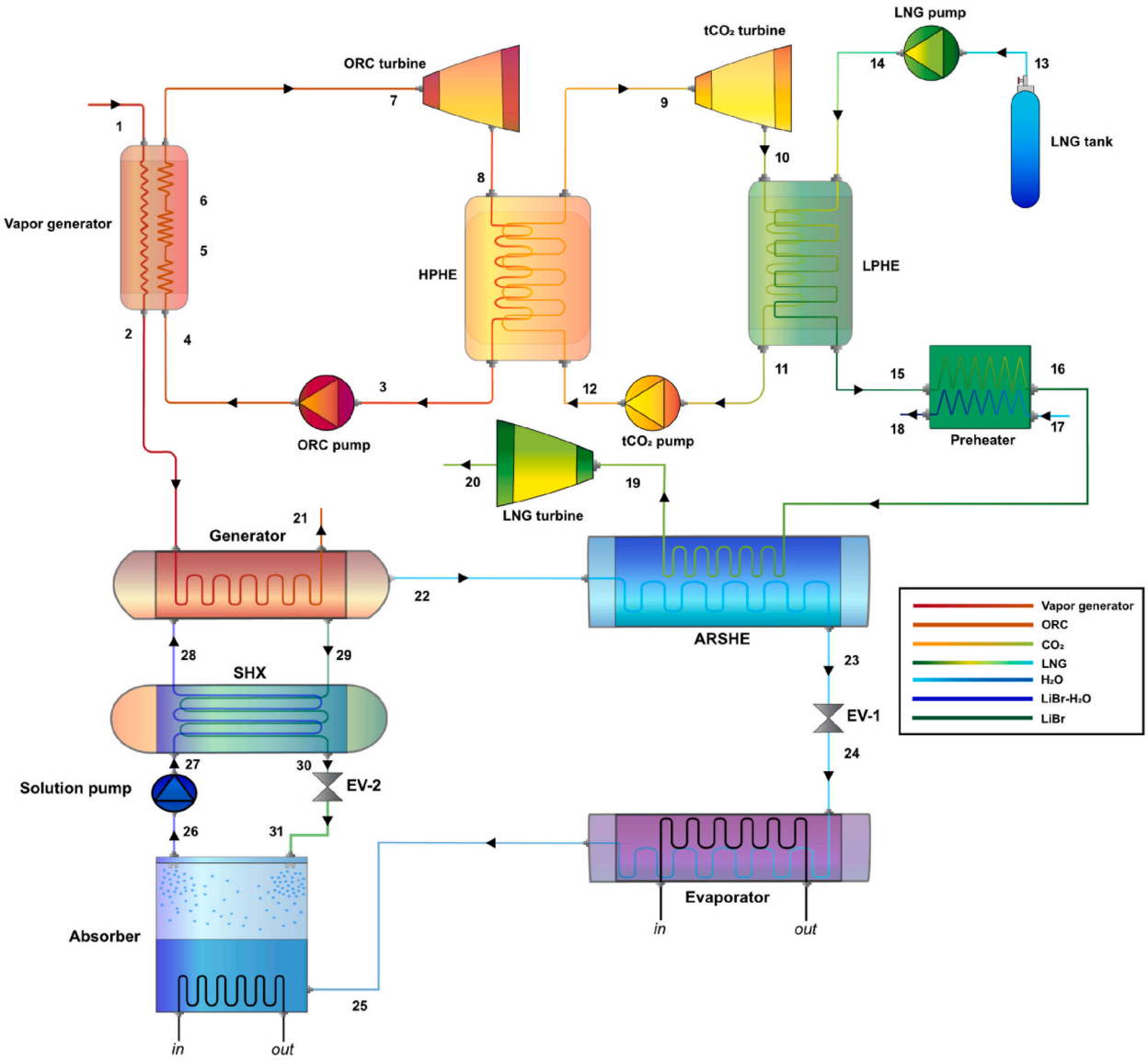

Fig. 3. Proposed ACPLU system.

valves. The integration is implemented using a heat exchanger between the generator and the outlet air stream of the vapor generator, where the outlet temperature of the vapor generator and a predetermined pinch temperature determines the generator outlet temperature. The same principle is used to enhance the LNG cold energy utilization. This is facilitated by the implementation of another heat exchanger (i.e., ARSHE) that takes advantage of the colder LNG stream to act as the condenser for the ARS.

After going through the vapor generator, the waste exhaust stream goes through another heat exchanger connected to the generator of the ARS. The heat extracted by the generator/heat exchanger is used to separate the binary mixture of LiBr and water. As mentioned before, water in the ARS system then goes through another heat exchanger (ARSHE), where the condensation process is facilitated by the cold LNG stream (state 22 to 23). As the enthalpy required in the condensation process is provided by the system itself, the cooling capacity, i.e., the COP, is likely to increase. Furthermore, the LNG stream temperature increases, which improves the work output from the LNG turbine. A tentative temperature-entropy (T-s) diagram for the proposed ACPLU system is shown in Fig. 4.

3. Selection of working fluids

A comparison analysis is conducted by choosing organic fluids to be used in the ORC of the ACPLU system. In this paper, pentane is selected as the working fluid for the ORC [5] and LiBr-water solution is used as the working fluid for the refrigeration cycle for the parametric analysis.

The performance of an ARS is also significantly influenced by the chemical and thermodynamic characteristics of its working fluid [47]. The combination of the absorbent and refrigerant must have a predetermined level of miscibility when operating in the temperature range in order to achieve optimal results [48]. Chemical inertness, non-explosiveness and non-toxicity is also favoured. Moreover, the evaporator temperature cannot be below the freezing point of water at a given pressure [49]. Some desirable characteristics of the ARS working fluid are: [50].

- The difference between the absorbent/refrigerant boiling temperatures should be high at a given pressure.

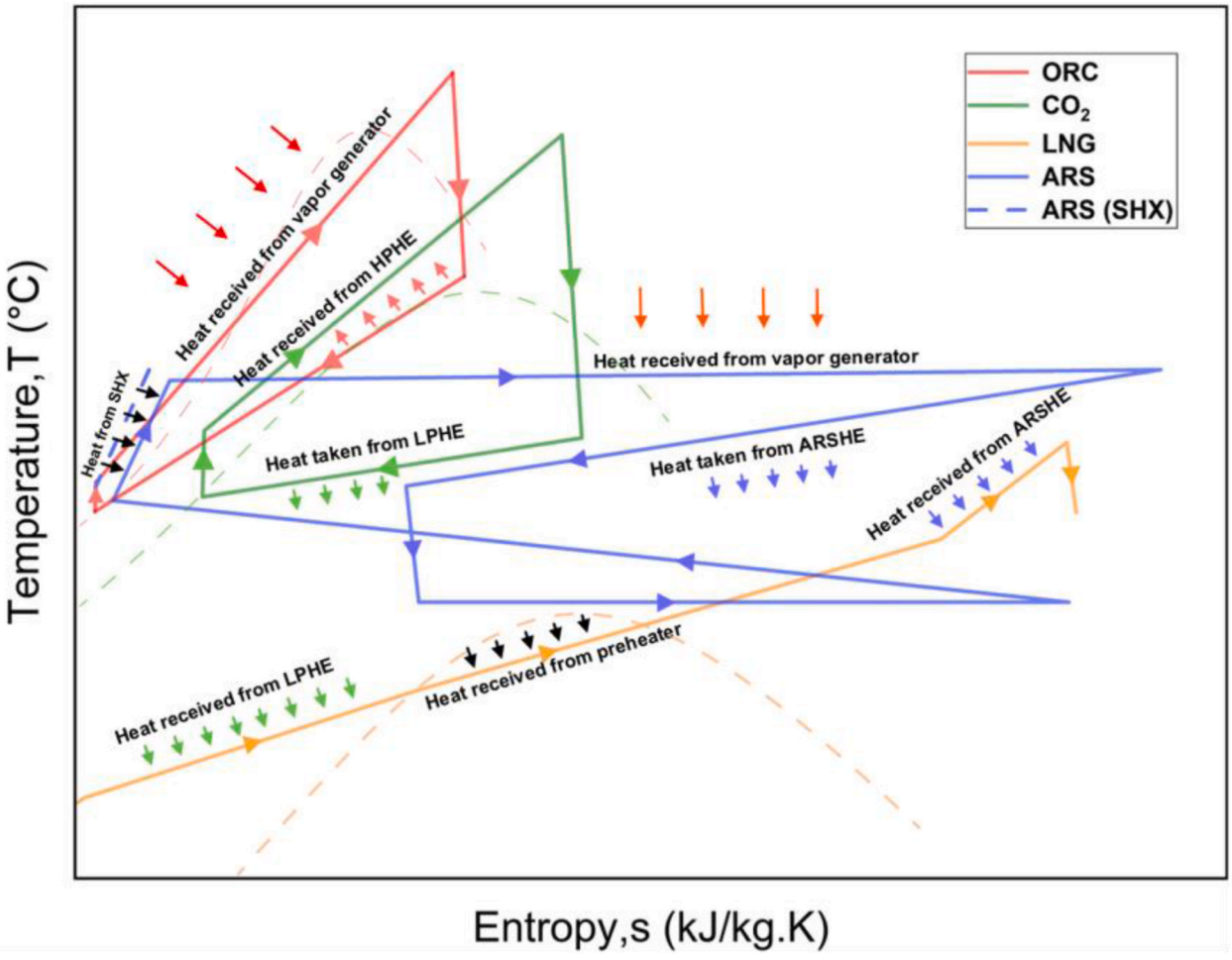

Fig. 4. Temperature-entropy (T-s) diagram for the proposed ACPLU system.

-A refrigerant with a high heat of vaporization.
-High LiBr concentration in the solution so that circulation ratio per unit of cooling capacity is low between the generator and the absorber.

As of today, 200 absorbent and 40 refrigerant compounds are available [51]. The most prevalent combinations used in ARSs are ammonia-water (NH_3–H_2O) and lithium bromide-water (LiBr–H_2O). NH_3–H_2O solution have had widespread applications in both heating and cooling. Ammonia-water has a large operating temperature range and boasts a high latent heat of vaporization that further facilitates effective system performance. Furthermore, ammonia's low specific volume and ability to operate at a high range of pressure means the ARS can be made more compact when using NH_3–H_2O.

However, NH_3–H_2O is less stable and usually requires a rectifier to separate water vapor from ammonia. This leads to increased heat loss, reduced efficiency, and introduces complexity to the cycle [52]. A significant drawback of using NH_3–H_2O solution is its inherent cytotoxicity. It's high working pressure range and corrosiveness, also limits the system's choice of material to corrosive resistant materials like carbon steel [53]. Conversely, the LiBr solution is more robust and cost-effective. The difference in boiling temperatures between LiBr and H_2O is higher, hence a rectifier is not necessary. However, the danger of crystallization of the solution limits it to operate in a narrow concentration range with an absorber temperature lower than approximately 40 °C [54].

4. Research methodology

4.1. Assumptions

The following assumptions taken from previous studies are used for the modelling of the ACPLU [5,55,56].

- Steady state conditions are maintained in all the systems.
- The waste stream that acts as the heat source is an ideal gas.
- Supercritical condition is assumed in the turbine inlet of the TCO_2 cycle, while superheated condition is assumed for the turbine inlet of the ORC.
- HPHE, LPHE, ARSHE outlet is always saturated liquid.
- The working fluid is in saturated liquid phase at the evaporator outlet.
- The working fluid is a weak solution at absorber outlet, at absorber temperature.
- The working fluid is a strong solution at generator outlet.
- Hydrostatic pressure and heat losses from the generator are at negligible levels.
- The exhaust air came out of the vapor generator at 100 °C and at 60 °C out of the generator.
- The isentropic efficiency for pumps and turbines is fixed at a constant value due to the inherent challenges associated with turbomachine modelling.
- The working fluid of the LNG stream is assumed to be methane.
- Working fluid through piping and condenser does not cause any pressure drop.
- Environmental condition is taken at 25 °C and 1 atm.
- The standard reference state for the International Institute of Refrigeration (IIR) is used ORC and LNG working fluids, and Normal Boiling Point (NBP) reference state was used for the TCO_2 cycle.

Steady state conditions allow for predictable and repeatable system performance. This is crucial for control, optimization, and safety in various engineering applications. Assuming steady-state conditions simplifies mathematical modelling and analysis. In many engineering applications, gases are approximated as ideal and pressure drop is neglected to streamline design and analysis. Moreover, assuming that the fluid comes out as a saturated liquid out of every condenser and the evaporator, the simplicity of the model is further enhanced. The assumption for taking a weak solution out of the evaporator outlet aligns with the thermodynamic equilibrium conditions. At the outlet of the absorber, the solution reaches a state where it has absorbed as much refrigerant vapor as it can at the given absorber temperature and pressure, forming a weak solution. Likewise, at the ARS generator outlet, the solution reaches a thermodynamic equilibrium where most of the refrigerant has been vaporized due to the applied heat, therefore producing a strong solution.

4.2. Thermodynamic energy equations

The mass, energy and exergy balance equations, along with the aforementioned assumptions, can be utilized to find the state properties of each of the components. The general form of the equations are as follows.

4.2.1. Integrated ORC-TCO_2-LNG system

The equations for the power cycle are taken from previous studies on cascaded ORC-TCO_2-LNG power cycles [5]. The temperature in the top cycle is considered superheated, so the temperature of the turbine inlet is given Equation (1):

$$T_{sup} = T_{eva} + \Delta t_{sup} \tag{1}$$

The steady flow energy balance formula shown in Equation (2) can be used to calculate the total energy throughout the system

[57].

$$\sum \dot{m}_{in}\left(h_{in}+\frac{V_{in}^2}{2}+gz_{in}\right)+\dot{Q}=\sum \dot{m}_{out}\left(h_{out}+\frac{V_{out}^2}{2}+gz_{out}\right)+\dot{W} \tag{2}$$

Where $\dot{m}$ is the mass flow rate, and h is the enthalpy of the stream at a specific state. $\dot{Q}$ and $\dot{W}$ is the energy associated with heat and work respectively. As the potential and kinetic energy of the flow is relatively negligible, the formula can be simplified as follows:

$$\sum \dot{m}_{in}h_{in}+\dot{Q}=\sum \dot{m}_{out}h_{out}+\dot{W} \tag{3}$$

Equation (4) is used to calculate power generation in the turbine:

$$\dot{W}_{tur}=\dot{m}_{in}\left(h_{in}-h_{out}\right) \tag{4}$$

where h_{out} can be found using the turbine efficiency formula shown in Equation (5):

$$\eta_{tur}=\frac{h_{in}-h_{out}}{h_{in}-h_{out,s}} \tag{5}$$

Power consumed by pump is calculated using Equation (6):

$$\dot{W}_{pump}=\dot{m}_{in}\left(h_{in}-h_{out}\right) \tag{6}$$

$\dot{W}_{pump}$ is negative as energy is consumed. The efficiency of the pump is given by Equation (7), which is used to find the outlet state properties of the pump, h_{out}

$$\eta_{pump}=\frac{h_{in}-h_{out,s}}{h_{in}-h_{out}} \tag{7}$$

The heat exchanger HPHE, LPHE, and ARSHE acts as the condenser for the higher temperature stream and as the boiler for the lower temperature stream (i.e., HPHE acts as the ORC condenser and as the boiler for the TCO_2 cycle). The temperature of the cold side outlet of the counter flow and parallel flow heat exchangers that are acting as condensers is given by Equation (8a) and Equation (8b) respectively:

$$T_{HE,cold\ side,out,CF}=T_{HE,hot\ side,in}-\Delta T_{pinch} \tag{8a}$$

$$T_{HE,cold\ side,out,PF}=T_{HE,hot\ side,out}-\Delta T_{pinch} \tag{8b}$$

The energy balance equation of the heat exchangers in Equation (9) is used to find the mass flow rate, given that enthalpy of the states is known.

$$\dot{m}_{wof,hot\ side}\left(h_{in}-h_{out}\right)=\dot{m}_{wof,cold\ side}\left(h_{in}-h_{out}\right) \tag{9}$$

The mass flow rate in the preheater is found using the following energy balance formula in Equation (10):

$$\dot{m}_{w}\left(h_{in}-h_{out}\right)=\dot{m}_{LNG}\left(h_{in}-h_{out}\right) \tag{10}$$

4.2.2. Refrigeration cycle

The waste heat exhaust, after passing through the power cycle, can be used to thermally drive the ARS. The heat from the waste gas can be correlated with the heat utilized by the generator of the ARS using Equation (11):

$$T_{gen}=T_{heat\ source,out}-\Delta T_{pinch,gen} \tag{11}$$

The components of the system can be assumed as a control volume. The continuity principle can be utilized to develop the mass balance equation:

$$\sum \dot{m}_{in}=\sum \dot{m}_{out} \tag{12}$$

The solution concentration balance is taken from a previous study on modified ARS [55]:

$$\sum \dot{m}_{in}X_{in}=\sum \dot{m}_{out}X_{out} \tag{13}$$

Heat absorbed or rejected by the components of the absorption refrigeration cycle is given by

$$\dot{Q}=\sum \dot{m}_{in}h_{in}-\sum \dot{m}_{out}h_{out} \tag{14}$$

As heat exchanger effectiveness has a significant effect on the cooling effect of the ARS, it was included during the modelling of the refrigeration cycle. The effectiveness can be explained as the ratio between the difference in temperature inlet and outlet on the hot side of the solution heat exchanger SHX and the absolute temperature difference of the working fluids that goes into the SHX. Equation (15) shows the effectiveness for the ARS preheater:

$$\xi = \frac{\Delta T_{SHX,\text{hot side}}}{\Delta T_{SHX,\text{in}}} \tag{15}$$

4.2.3. Overall proposed CCP system

Finally, the net power output of the ACPLU system can be computed by finding the sum total of the power produced and consumed in the ORC, TCO_2, LNG turbine and ORC, TCO_2, LNG, and ARS pump, respectively, as shown in.

$$\dot{W}_{net} = \sum \dot{W}_{tur} - \sum \dot{W}_{pump} \tag{16}$$

The following obtains the COP for refrigeration of the ACPLU:

$$COP_{heating} = \frac{Q_{eva}}{Q_{gen} + \dot{W}_{pump,ARS}} \tag{17}$$

But as the work done by the ARS pump is negligible compared to the power input by the generator, the equation is simplified as follows:

$$COP_{heating} = \frac{Q_{eva}}{Q_{gen}} \tag{18}$$

4.3. Exergy analysis

The maximum net work output from a system from a specific state to a reference state (usually the state of its surrounding) is called exergy. The exergy of a control volume is computed using the following equation:

$$\dot{E}^{Q} + \sum \dot{m}_{in} e_{in} = \dot{E}^{W} + \sum \dot{m}_{out} e_{out} + \dot{E}^{D} \tag{19}$$

$\dot{E}^{Q}$ represents the exergy associated with heat transfer:

$$\dot{E}^{Q} = \left(1 - \frac{T_0}{T_r}\right) \tag{20}$$

$\dot{E}^{W}$ represents the exergy associated with work:

$$\dot{E}^{W} = \dot{W} \tag{21}$$

Exergy transfer through mass transfer is found using Equation (22):

$$\dot{E} = \dot{m}e \tag{22}$$

Where e is the specific exergy. The specific exergy can be divided into four subcategories: kinetic, potential, physical and chemical exergy as shown below:

$$e = e_{ki} + e_{po} + e_{ph} + e_{ch} \tag{23}$$

Due to negligible changes in the kinetic and potential exergy, the first two terms can be assumed negligible. Moreover, as the proposed system does not involve any chemical reactions, the chemical exergy can also be deemed negligible. Hence, the exergy transfer equation is simplified and expanded to Equation (24):

$$e = (h - h_0) - T_0(s - s_0) \tag{24}$$

The exergy destruction is the exergy used up by a component of a system. The general exergy destruction equation of each component is given in Table 1.

For the ACPLU system, the net rate of the exergy input is the summation of the exergy input from the heat source and the LNG stream, as shown in Equation (25). This is primarily due to the LNG stream having an abundance of chemical exergy that can be used be

Table 1
Exergy destruction of each component in the system.

Component	Exergy destruction
Vapor generator	$\dot{E}^{D}_{VG} = \sum \dot{E}_{in} - \sum \dot{E}_{out}$
Turbine	$\dot{E}^{D}_{tur} = \dot{E}_{in} - \dot{E}_{out} - \dot{W}_{tur}$
Pump	$\dot{E}^{D}_{pump} = \dot{E}_{in} - \dot{E}_{out} + \dot{W}_{pump}$
Condenser/Heat exchanger; Generator; Evaporator; Absorber	$\dot{E}^{D}_{HPHE} = \dot{E}^{D}_{LPHE} = \dot{E}^{D}_{ARSHE} = \dot{E}^{D}_{SHX} = \dot{E}^{D}_{gen} = \dot{E}^{D}_{evp} = \dot{E}^{D}_{abs} = \sum \dot{E}_{in} - \sum \dot{E}_{out}$
Preheater	$\dot{E}^{D}_{preheater} = \sum \dot{E}_{in} - \sum \dot{E}_{out}$

utilized in some other process [5].

$$\dot{E}_{in,power\ \&\ refrigeration} = \dot{E}_{heat\ source} + \dot{E}_{LNG} \tag{25}$$

Where the rate of exergy from is heat source in calculated using Equation (26):

$$\dot{E}_{heat\ source} = Q_{in,heat\ source} \times \left(1 - \frac{T_0}{T_{heat\ source,in}}\right) \tag{26}$$

The exergy input from the LNG stream, which is the exergy rate between the inlet and outlet of the LNG system, is calculated using Equation (27):

$$\dot{E}_{LNG} = \dot{E}_{LNG,in} - \dot{E}_{LNG,out} \tag{27}$$

The net rate of useful exergy by the ACPLU system can also be divided into three categories: (a) The net work done by the proposed system; (b) The useful exergy developed in the form of cooling by the ARS evaporator and (c) The useful exergy in the form of chilled water in the water chiller. The useful exergy developed by the ARS evaporator and the preheater is given by Equation (28) and Equation (29) respectively:

$$\dot{E}_{ARS} = \left|\dot{Q}_{evp} \times \left(1 - \frac{T_0}{T_{evp}}\right)\right| \tag{28}$$

$$\dot{E}_{preheater} = \left|\dot{E}_{w,in} - \dot{E}_{w,out}\right| \tag{29}$$

Finally, second law efficiency of the combined cycle is calculated using Equation (30):

$$\psi = \frac{\dot{E}_{ARS} + \dot{W}_{net} + \dot{E}_{water\ chiller}}{\dot{E}_{in,power\ \&\ refrigeration}} \times 100\% \tag{30}$$

4.4. Thermo-economic analysis

After confirming the thermodynamic viability of the system, assessing its economic feasibility requires determining its implementation costs. Usually, the cost of implementing such a system consists of capital investments, and the operation and maintenance costs of the system over a period of time. The cost function equations of the thermodynamic components, $Z_{components}$, which is the capital needed to acquire the components according to the boundary conditions and performance (power output and/or input) is shown in Table 2. Here, the capital cost of the ARS components, excluding the solution pump, has been taken from the study undertaken by Wang et al. [41], using a reference heat transfer area of 100 m^2 and the reference capital cost values given in Table 3. The basic cost data of the ARS component at 2000 is transferred to the 2018 cost data using the Chemical Engineering Plant Cost Index (CEPCI) values shown in Table 8.

Using the heat transfer coefficient values given in Table 8, the heat transfer area is found using Equation (31):

$$A_{component} = \frac{hot\ side(h_{in} - h_{out})}{U \times \Delta T_{LMTD}} \tag{31}$$

Where U is the heat transfer coefficient and ΔT_{LMTD}, is the logarithmic mean temperature difference, given by Equation (32a) and Equation (32b) for counter flow and parallel flow heat exchangers respectively:

Table 2
Capital cost function equation of the components in the ACPLU system [15,41,58].

Components	Capital cost function of the system component
Vapor generator, HPHE, LPHE	$Z_{vapor\ generator/HPHE/LPHE} = 2681 \times A_{component}^{0.59}$
Preheater	$Z_{preheater} = 1397 A_{preheater}^{0.89}$
ORC/TCO_2/LNG turbine	$Z_{ORC/TCO_2/LNG_{tur}} = 4405 \dot{W}_{tur}^{0.89}$
ORC/TCO_2/LNG/solution pump	$Z_{ORC/TCO_2/LNG/solution_{pump}} = 3540 \dot{W}_{pump}^{0.7}$
Generator, ARSHE, evaporator, absorber, SHX	$Z_{gen/ARSHE/evp/abs/SHX} = Z_{ref,component}\left(\frac{A_{component}}{A_{ref}}\right)^{0.6} \times \frac{CEPCI_{2018}}{CEPCI_{2000}}$
EV1, EV2	$Z_{EV1/EV2} = Z_{ref,component} \times \frac{CEPCI_{2018}}{CEPCI_{2000}}$

[a] $A_{ref} = 100\ m^2$.
[b] Z_{ref} = Table 3.
[c] $CEPCI_{2018} = 638.1$
[d] $CEPCI_{2000} = 394.1$

Table 3
Reference capital cost of ARS components [41].

Components	Capital cost ($)
Generator	17,500
ARSHE	8000
Evaporator	16,000
Absorber	16,500
SHX	12,000
EV1, EV2	300

The capital cost recovery function, *CRF,* is determined using Equation (33).

$$\Delta T_{LMTD\,CF} = \frac{T_{hot\ side,in} - T_{cold\ side,out} + T_{hot\ side,out} - T_{cold\ side,in}}{\ln\left(\frac{T_{hot\ side,in} - T_{cold\ side,out}}{T_{hot\ side,out} - T_{cold\ side,in}}\right)} \tag{32a}$$

$$\Delta T_{LMTD\,PF} = \frac{T_{hot\ side,in} - T_{cold\ side,in} + T_{hot\ side,out} - T_{cold\ side,out}}{\ln\left(\frac{T_{hot\ side,in} - T_{cold\ side,in}}{T_{hot\ side,out} - out}\right)} \tag{32b}$$

The logarithmic mean temperature difference of the generator, evaporator and absorber is given in Table 8.

$$CRF = \frac{i_r(1+i_r)^n}{(1+i_r)^n - 1} \tag{33}$$

where i_r is the interest rate, and n is the years of operation of the ACPLU.

The cost rate for a component, $\dot{Z}_{component}$, is given by Equation (34):

$$\dot{Z}_{component} = \left(\frac{CRF \times \gamma_k}{\tau}\right) Z_{component} \tag{34}$$

Where γ_k is the maintenance factor to consider the costs of operation and maintenance, and τ denotes the annual hours of operation of the ACPLU.

Finally, the average cost per unit of useful energy is calculated using Equation (35):

Table 4
Governing mass, temperature, and energy balance equations for the cascaded power cycle.

Component	Mass balance	Temperature balance	Energy balance
Vapor generator	$\dot{m}_1 = \dot{m}_2$ $\dot{m}_4 = \frac{\dot{m}_1(h_1 - h_2)}{h_7 - h_4}$ $\dot{m}_4 = \dot{m}_5 = \dot{m}_6 = \dot{m}_7$	$T_7 = T_6 + \Delta T_{sup}$	$Q_{in,heat\ source} = \dot{m}_1(T_1 - T_2)$
ORC turbine	$\dot{m}_7 = \dot{m}_8$	-	$\dot{W}_{tur,ORC} = \dot{m}_7(h_7 - h_8)$
HPHE	$\dot{m}_8 = \dot{m}_3$ $\dot{m}_9 = \frac{\dot{m}_8(h_8 - h_3)}{h_9 - h_{12}}$ $\dot{m}_9 = \dot{m}_{12}$	$T_9 = T_8 - \Delta T_{pinch,HPHE}$	$Q_{HPHE} = \dot{m}_8(h_3 - h_8)$
ORC pump	$\dot{m}_3 = \dot{m}_4$	-	$\dot{W}_{pump,ORC} = \dot{m}_3(h_4 - h_3)$
CO_2 turbine	$\dot{m}_9 = \dot{m}_{10}$	-	$\dot{W}_{tur,CO_2} = \dot{m}_9(h_9 - h_{10})$
LPHE	$\dot{m}_{10} = \dot{m}_{11}$ $\dot{m}_{14} = \frac{\dot{m}_{11}(h_{10} - h_{11})}{h_{15} - h_{14}}$ $\dot{m}_{14} = \dot{m}_{15}$	$T_{15} = T_{11} - \Delta T_{pinch,LPHE}$	$Q_{LPHE} = \dot{m}_{10}(h_{10} - h_{11})$
CO_2 pump	$\dot{m}_{11} = \dot{m}_{12}$	-	$\dot{W}_{pump,CO_2} = \dot{m}_{11}(h_{12} - h_{11})$
LNG pump	$\dot{m}_{13} = \dot{m}_{14}$	-	$\dot{W}_{pump,LNG} = \dot{m}_{13}(h_{14} - h_{13})$
Preheater	$\dot{m}_{15} = \dot{m}_{16}$ $\dot{m}_{16} = \frac{\dot{m}_{15}(h_{18} - h_{15})}{h_{16} - h_{17}}$ $\dot{m}_{17} = \dot{m}_{18}$	$T_{18} = T_{16} - \Delta T_{pinch,preheater}$	$Q_{preheater} = \dot{m}_{17}(h_{17} - h_{18})$
LNG turbine	$\dot{m}_{16} = \dot{m}_{19}$	-	$\dot{W}_{tur,LNG} = \dot{m}_{16}(h_{16} - h_{19})$

*The state points in this table corresponds to the state points of the system depicted in Fig. 1.

$$c_{ACPLU} = \frac{\sum_{component}^{N} \dot{Z}_{component}}{\dot{W}_{net} + Q_{eva}} \times \frac{1000000}{3600} \tag{35}$$

Where N is the total number of components.

5. Mathematical modelling

The components are computed as a control volume, using the assumptions given in **4.1. Assumptions**. The temperature, mass, energy balance equations for the standalone power cycle and ARS are given in Tables 4 and 5 respectively. Table 6 represents the equations for temperature, mass, and energy balance for the ACPLU with state points corresponding to Fig. 3. Additionally, the equations for exergy destruction rate for the ACPLU system are shown in Table 7.

The mathematical modelling chronology is followed in the way shown in Fig. 5. Thermodynamic properties of all the working fluids are taken from the EES library and the program is simulated using the operating parameters depicted in Table 8. The operating parameters are taken after careful deliberations of the operating parameters used in previous studies [5,19,41,55,58,59]. The difference in operating temperature range between the LPHE, streams is kept to an absolute minimum and the supercritical condition of the LPHE outlet means that effectiveness of the heat exchanger is high [5]. The range of T_{gen} and the assumed value of T_{abs} is taken in a way that crystallization of the working fluid does not occur [55]. The evaporator temperature, T_{evp} is assumed to be 5 °C. Even though the evaporator temperature is below the melting temperature of water, it can still be assumed that water stays in liquid phase. This is because, as the water is moving at a very low mass flow rate, the water can be assumed to be a bulk liquid. Bulk water is reported to freeze with temperatures below −30 °C [60] which can only be increased to the range of −8 °C to −15 °C using ice-binding surfaces. Furthermore, water in small spaces composed of minerals (i.e., pipes), is observed to freeze below 0 °C [61]. Even so, freezing of water may occur if an evaporator temperature around −30°C is taken. Nevertheless, to prevent the possibility for the water to even freeze partially, a minimum evaporator temperature of −5 °C is taken. By addressing these assumptions and their impacts, we tried to provide a clearer understanding of the potential limitations of our study. We acknowledge that these assumptions introduce certain constraints and potential deviations which can be validated with sensitivity analysis in future to refine the model and ensure its robustness in real-world applications.

6. Multi-objective optimization (MOO)

Finding the proper combination of operating parameters is pertinent with overall system performance. Multi-objective optimization (MOO) can help in finding the suitable combination of operating parameters that favors one or multiple aspects of system performance, i.e., net work output or 2nd law efficiency, or both. In this paper, MOO is conducted using the steps shown in Fig. 6. The different sections used in the MOO are discussed below.

6.1. Artificial neural network (ANN) model

Artificial neural networks (ANNs) are used to form a parametric model, that is regulated by trainable parameters, by using a large set of trainable data. This parametric model can be used to predict the values of unknown parameters, in between and even outside the dataset range, classify patterns, categorize, as well as functionalize a set of data [62]. ANNs are based on the nerve call or neuron (hence, the name Artificial *Neural* Network). Just like the biological nerve cell, a neuron of the ANN gets a multitude of inputs from other neurons, and based on the weighted total of the inputs, the output is either 0 or 1 [63]. The back-propagation learning algorithm in MATLAB 2021b (MathWorks, Massachusetts, United States) was used to acquire the objective function. A visual depiction of an ANN

Table 5
Governing mass, temperature, and energy balance equations for ARS system.

Component	Mass balance	Temperature balance	Energy balance
Generator	$\dot{m}_1 = \dot{m}_{gen}$ $\dot{m}_7 = \dot{m}_1 + \dot{m}_8$ $\dot{m}_8 = \frac{\dot{m}_1 x_7}{x_8 - x_7}$	$T_1 = T_{gen}$ $T_8 = T_{gen}$	$h_7 = h_6 + \left(\frac{\dot{m}_8}{\dot{m}_7}.h_8 - \frac{\dot{m}_9}{\dot{m}_7}.h_9\right)$ $Q_{gen} = \dot{m}_1 h_1 + \dot{m}_8 h_8 - \dot{m}_7 h_7$
Condenser	$\dot{m}_2 = \dot{m}_1$	$T_2 = T_{cond}$	$Q_{cond} = \dot{m}_1(h_1 - h_2)$
EV-1	$\dot{m}_3 = \dot{m}_1$		-
Evaporator	$\dot{m}_4 = \dot{m}_1$	$T_4 = T_{evp}$	$h_3 = h_2$ $Q_{evp} = \dot{m}_4(h_4 - h_3)$
Absorber	-	$T_5 = T_{abs}$	$Q_{abs} = \dot{m}_4 h_4 + \dot{m}_{10} h_{10} - \dot{m}_5 h_5$
SHX	$\dot{m}_6 = \dot{m}_7$ $\dot{m}_9 = \dot{m}_8$	$T_9 = T_8 - \xi(T_8 - T_6)$	-
EV-2	$\dot{m}_{10} = \dot{m}_9$	$T_{10} = T_9$	$h_{10} = h_9$
Solution pump	$\dot{m}_5 = \dot{m}_6$	$T_6 = T_5$	$h_6 = h_5$ $\dot{W}_{pump,ARS} = \dot{m}_5(h_6 - h_5)$

*The state points correspond to the state points for the system depicted in Fig. 2.

Table 6
Governing mass, temperature, and energy balance equations for the proposed CCP system.

Component	Mass balance	Temperature balance	Energy balance
Vapor generator	$\dot{m}_1 = \dot{m}_2$ $\dot{m}_4 = \frac{\dot{m}_1(h_1 - h_2)}{h_7 - h_4}$ $\dot{m}_4 = \dot{m}_5 = \dot{m}_6 = \dot{m}_7$	$T_7 = T_6 + \Delta T_{sup}$	$Q_{in,heat\ source} = \dot{m}_1(T_1 - T_{21})$
ORC turbine	$\dot{m}_7 = \dot{m}_8$	-	$\dot{W}_{tur,ORC} = \dot{m}_7(h_7 - h_8)$
HPHE	$\dot{m}_8 = \dot{m}_3$ $\dot{m}_9 = \frac{\dot{m}_8(h_8 - h_3)}{h_9 - h_{12}}$ $\dot{m}_9 = \dot{m}_{12}$	$T_9 = T_8 - \Delta T_{pinch,HPHE}$	$Q_{HPHE} = \dot{m}_8(h_3 - h_8)$
ORC pump	$\dot{m}_3 = \dot{m}_4$	-	$\dot{W}_{pump,ORC} = \dot{m}_3(h_4 - h_3)$
CO_2 turbine	$\dot{m}_9 = \dot{m}_{10}$	-	$\dot{W}_{tur,CO_2} = \dot{m}_9(h_9 - h_{10})$
LPHE	$\dot{m}_{10} = \dot{m}_{11}$ $\dot{m}_{14} = \frac{\dot{m}_{11}(h_{10} - h_{11})}{h_{15} - h_{14}}$ $\dot{m}_{14} = \dot{m}_{15}$	$T_{15} = T_{11} - \Delta T_{pinch,LPHE}$	-
CO_2 pump	$\dot{m}_{11} = \dot{m}_{12}$	-	$\dot{W}_{pump,CO_2} = \dot{m}_{11}(h_{12} - h_{11})$
LNG pump	$\dot{m}_{13} = \dot{m}_{14}$	-	$\dot{W}_{pump,LNG} = \dot{m}_{13}(h_{14} - h_{13})$
Preheater	$\dot{m}_{15} = \dot{m}_{16}$ $\dot{m}_{16} = \frac{\dot{m}_{15}(h_{18} - h_{15})}{h_{16} - h_{17}}$ $\dot{m}_{17} = \dot{m}_{18}$	$T_{18} = T_{16} - \Delta T_{pinch,preheater}$	$Q_{preheater} = \dot{m}_{17}(h_{17} - h_{18})$
ARSHE (cold side)	$\dot{m}_{16} = \dot{m}_{19}$	$T_{19} = T_{18} + \Delta T_{pinch,ARSHE}$	-
LNG turbine	$\dot{m}_{20} = \dot{m}_{19}$	-	$\dot{W}_{tur,LNG} = \dot{m}_{19}(h_{19} - h_{20})$
Generator	$\dot{m}_{21} = \dot{m}_1$ $\dot{m}_{22} = \dot{m}_{gen}$ $\dot{m}_{28} = \dot{m}_{22} + \dot{m}_{29}$ $\dot{m}_{29} = \frac{\dot{m}_{22}x_{28}}{x_{29} - x_{28}}$	$T_{gen} = T_2 - \Delta T_{pinch,gen}$ $T_{22} = T_{gen}$ $T_{29} = T_{gen}$	$h_{28} = h_{27} + \left(\frac{\dot{m}_{29}}{\dot{m}_{28}}.h_{29} - \frac{\dot{m}_{30}}{\dot{m}_{28}}.h_{30}\right)$ $Q_{gen} = \dot{m}_{22}h_{22} + \dot{m}_{29}h_{29} - \dot{m}_{28}h_{28}$
ARSHE (hot side)	$\dot{m}_{23} = \dot{m}_{22}$	$T_{23} = T_{cond}$	$Q_{cond} = \dot{m}_{22}(h_{22} - h_{23})$
EV-1	$\dot{m}_{24} = \dot{m}_{23}$	-	$h_{24} = h_{23}$
Evaporator	$\dot{m}_{25} = \dot{m}_{24}$	$T_{25} = T_{evp}$	$Q_{evp} = \dot{m}_{25}(h_{25} - h_{24})$
Absorber	$\dot{m}_{26} = \dot{m}_{25}$	$T_{26} = T_{abs}$	$Q_{abs} = \dot{m}_{25}h_{25} + \dot{m}_{31}h_{31} - \dot{m}_{26}h_{26}$
SHX	$\dot{m}_{27} = \dot{m}_{28}$ $\dot{m}_{30} = \dot{m}_{29}$	$T_{30} = T_{29} - \xi(T_{29} - T_{27})$	-
EV-2	$\dot{m}_{31} = \dot{m}_{30}$	$T_{31} = T_{30}$	$h_{31} = h_{30}$
Solution pump	$\dot{m}_{27} = \dot{m}_{26}$	$T_{27} = T_{26}$	$h_{27} = h_{26}$ $\dot{W}_{pump,ARS} = \dot{m}_{26}(h_{27} - h_{26})$

* The state points correspond to the state points for the system depicted in Fig. 3.

with back-propagation learning is shown in Fig. 7.

A dataset of 1188 observations with 3 inputs and 2 outputs is used. The data vision is set randomly, and the Bayesian regularization training algorithm is employed with a hidden layer size of 27. Among available training algorithms, Bayesian regularization training algorithm is chosen for better generalization of the data. The cost function: Mean Squared Error is calculated using **Equation (36)**, to find the accuracy of the trained model [64].

$$MSE = \frac{1}{N}\sum_{n=1}^{N}(y_n - t_n)^2 \tag{36}$$

Where t_n, y_n are the real and predicted value respectively and N is the number of data.

6.2. *Multi-objective optimization genetic algorithm (GA)*

The capability of solving incredibly complex and nonlinear problems with a relatively low computational power requirement makes the genetic algorithm (GA) a very useful tool [65]. Integrating ANN before finding the optimal solution with GA reduces the computation time substantially [66]. This makes the GA an ideal choice for the optimization of thermodynamic systems [64]. Using the upper and lower constraints of the input parameters shown in Table 9 and the GA parameters shown in Table 10, a multi-objective optimization was conducted using the *gamultiobj* solver in MATLAB 2021b (MathWorks, Massachusetts, United States) for the combinations of input parameters for (A) Maximum net work output; (B) Optimal point and (C) Maximum second law efficiency. The other GA parameters were kept in default settings.

7. Model validation

Due to the novelty of the ACPLU system, the mathematical model cannot be validated using existing systems in the literature. The

Table 7
Exergy destruction equations for the proposed CCP system.

Component	Exergy destruction
Vapor generator	$\dot{E}^D_{VG} = \dot{E}_1 - \dot{E}_2 + \dot{E}_4 - \dot{E}_7 = = [\dot{m}_1\{(h_1 - h_2) - T_0(s_1 - s_2)\}] + [\dot{m}_4\{(h_4 - h_7) - T_0(s_4 - s_7)\}]$
ORC turbine	$\dot{E}^D_{tur,ORC} = \dot{E}_7 - \dot{E}_8 - \dot{W}_{tur,ORC} = \dot{m}_7 T_0(s_8 - s_7)$
HPHE	$\dot{E}^D_{HPHE} = \dot{E}_8 - \dot{E}_3 + \dot{E}_{12} - \dot{E}_9 = [\dot{m}_8\{(h_8 - h_3) - T_0(s_8 - s_3)\}] + [\dot{m}_{12}\{(h_{12} - h_9) - T_0(s_{12} - s_9)\}]$
ORC pump	$\dot{E}^D_{pump,ORC} = \dot{E}_3 - \dot{E}_4 + \dot{W}_{pump,ORC} = \dot{m}_4 T_0(s_4 - s_3)$
CO_2 turbine	$\dot{E}^D_{tur,CO_2} = \dot{E}_9 - \dot{E}_{10} - \dot{W}_{tur,CO_2} = \dot{m}_9 T_0(s_{10} - s_9)$
LPHE	$\dot{E}^D_{LPHE} = \dot{E}_{10} - \dot{E}_{11} + \dot{E}_{14} - \dot{E}_{15} = [\dot{m}_{10}\{(h_{10} - h_{11}) - T_0(s_{10} - s_{11})\}] + [\dot{m}_{14}\{(h_{14} - h_{15}) - T_0(s_{14} - s_{15})\}]$
CO_2 pump	$\dot{E}^D_{pump,CO_2} = \dot{E}_{11} - \dot{E}_{12} + \dot{W}_{pump,CO_2} = \dot{m}_{11} T_0(s_{12} - s_{11})$
LNG pump	$\dot{E}^D_{pump,LNG} = \dot{E}_{13} - \dot{E}_{14} + \dot{W}_{pump,LNG} = \dot{m}_{13} T_0(s_{14} - s_{13})$
Preheater	$\dot{E}^D_{preheater} = \dot{E}_{15} - \dot{E}_{16} + \dot{E}_{17} - \dot{E}_{18} = [\dot{m}_{15}\{(h_{15} - h_{16}) - T_0(s_{15} - s_{16})\}] + [\dot{m}_{17}\{(h_{17} - h_{18}) - T_0(s_{17} - s_{18})\}]$
ARSHE	$\dot{E}^D_{ARSHE} = \dot{E}_{16} - \dot{E}_{19} + \dot{E}_{22} - \dot{E}_{23} = [\dot{m}_{16}\{(h_{16} - h_{19}) - T_0(s_{16} - s_{19})\}] + [\dot{m}_{22}\{(h_{22} - h_{23}) - T_0(s_{22} - s_{23})\}]$
LNG turbine	$\dot{E}^D_{tur,LNG} = \dot{E}_{19} - \dot{E}_{20} - \dot{W}_{tur,LNG} = \dot{m}_{19} T_0(s_{20} - s_{19})$
Generator	$\dot{E}^D_{gen} = \dot{E}_2 - \dot{E}_{21} - \dot{E}_{22} + \dot{E}_{28} - \dot{E}_{29} = \dot{m}_2\{(h_2 - h_{23}) - T_0(s_2 - s_{23})\} - \dot{m}_{22}\{(h_{22} - h_0) - T_0(s_{22} - s_0)\} + \dot{m}_{28}\{(h_{28} - h_0) - T_0(s_{28} - s_0)\} - \dot{m}_{29}\{(h_{29} - h_0) - T_0(s_{29} - s_0)\}$
EV-1	$\dot{E}^D_{EV-1} = \dot{E}_{23} - \dot{E}_{24} = \dot{m}_{23}\{(h_{23} - h_{24}) - T_0(s_{23} - s_{24})\}$
Evaporator	$\dot{E}^D_{evp} = \dot{E}_{24} - \dot{E}_{25} = \dot{m}_{24}\{(h_{24} - h_{25}) - T_0(s_{24} - s_{25})\}$
Absorber	$\dot{E}^D_{abs} = \dot{E}_{25} + \dot{E}_{31} - \dot{E}_{26} = \dot{m}_{25}\{(h_{25} - h_0) - T_0(s_{25} - s_0)\} + \dot{m}_{31}\{(h_{31} - h_0) - T_0(s_{31} - s_0)\} - \dot{m}_{26}\{(h_{26} - h_0) - T_0(s_{26} - s_0)\}$
SHX	$\dot{E}^D_{SHX} = \dot{E}_{27} - \dot{E}_{28} + \dot{E}_{29} - \dot{E}_{30} = \dot{m}_{27}\{(h_{27} - h_{28}) - T_0(s_{27} - s_{28})\} + [\dot{m}_{29}\{(h_{29} - h_{30}) - T_0(s_{29} - s_{30})\}]$
EV-2	$\dot{E}^D_{EV-2} = \dot{E}_{30} - \dot{E}_{31} = \dot{m}_{30}\{(h_{30} - h_{31}) - T_0(s_{30} - s_{31})\}$
Solution pump	$\dot{E}^D_{pump,ARS} = \dot{E}_{26} - \dot{E}_{27} + \dot{W}_{pump,ARS} = \dot{m}_{26} T_0(s_{27} - s_{26})$

* The state points correspond to the state points for the system depicted in Fig. 3.

different sub-systems, however, are validated against existing literature. The power cycle is modelled and validated against the previous study on the double cascade ORC-TCO$_2$-LNG cycle proposed by Sadreddini et al. [5] and the refrigeration cycle is validated against the single-effect ARS proposed by Modi et al. [56], as shown in Fig. 8 and Table 11.

The results indicate that the parameters chosen for the validation of the ARS are highly consistent with the previous study, with a maximum error having a value of only 0.57 %. However, for the power cycle, the work output from the LNG cycle shows a significant error of 4.85 % between the reference and simulated model. This discrepancy in the LNG cycle's performance stems from the previous study only accounting for pressure drop within the LNG cycle. Even though our mathematical model accounts for that pressure drop, there are still differences in the state values for the LNG cycle. Another possible reason could be the differences in the library used. In our study, we have modelled the system with Engineering Equation Solver (EES), using the integrated fluid property library to find the state properties of the cycle, while the system for the reference study was developed in MATLAB and used fluid properties from the REFPROP library [67]. Here, the fluid property of methane (the chosen working fluid for the LNG cycle) differed between the two libraries. Nevertheless, aggregating the work output from each cycle to find the net work done, the error between the reference model and simulated model reduced to 0.94 %, concluding that the power cycle is also highly consistent.

8. Results and discussion

The computed state properties with pentane as the ORC working fluid are presented in Table 12. Using the assumed parameters, outlined in Table 8, a second law efficiency of 27.3 %, a net work output of 11.761 MW, and a COP of 0.7403 is achieved. Pentane is chosen as it shows one of the highest exergy efficiencies among the organic fluids that are tested for a comparative thermal analysis (shown in Table 12). Moreover, a sensitivity analysis is performed by varying several operating parameters to evaluate the effect on performance metrics such as: net work by each cycle, mass flow rates, COP, second law efficiency, exergy destruction as well as heat absorbed by the evaporator of the ARS. Finally, multi-objective optimization is conducted to identify combinations that yield the highest second law efficiency, highest net work done, and an optimal performance.

8.1. Comparison of working fluids in the ORC

The choice of the ORC working fluid significantly impacts the performance of the ACPLU system. For this study, 10 organic fluids were selected to compare their effects on overall system performance, as shown in Table 13, detailing their thermodynamic properties. Environmentally unsuitable refrigerant such as R11, R12, R113, R114, etc. was not chosen as part of the study. Table 14 shows the computed net work, first and second law efficiency of the ACPLU with different working fluid in the ORC. As the turbine inlet pressures of the ORC changes with its working fluid, a default value for each working fluid is chosen to be the nearest whole number below its corresponding critical pressure. It is observed that the degree of superheating provides a limiting factor to the maximum temperature allowed by the ORC. Hence, the optimum temperature of 28.1 °C is used for all the working fluids. Likewise, a pressure of 1.4653 bar is

Table 8
Assumptions and values used for simulation [5,19,41,55,58,59].

Parameter	*Formula*	Unit	Value
Reference temperature (ambient)	T_0	°C	25
Reference pressure (ambient)	P_0	bar	1.01
Heat source inlet temperature	T_1	°C	300
Heat source outlet temperature	T_2	°C	100
Temperature of exhaust gas after passing ARS generator	T_{21}	°C	60
Heat source mass flow rate	$\dot{m}_1$	kg/s	120
ARS mass flow rate	$\dot{m}_{22}$	kg/s	1
ORC turbine inlet pressure	P_7	bar	33
ORC condenser pressure	P_8	bar	1.4653
TCO_2 turbine inlet pressure	P_9	bar	80.13
TCO_2 condenser pressure	P_{10}	bar	6
Isentropic efficiency of turbine	η_{tur}	%	85
Isentropic efficiency of pump	η_{pump}	%	75
LNG inlet temperature	T_{13}	°C	−161.7
LNG inlet pressure	P_{13}	bar	1.01
LNG turbine outlet pressure	P_{20}	bar	40
Superheated temperature	ΔT_{sup}	°C	28.1
Pinch temperature in HPHE	$\Delta T_{pinch,HPHE}$	°C	8
Pinch temperature in LPHE	$\Delta T_{pinch,LPHE}$	°C	50
Pinch temperature in preheater	$\Delta T_{pinch,preheater}$	°C	50
Pinch temperature in ARSHE	$\Delta T_{pinch,ARSHE}$	°C	50
Pinch temperature in generator heat exchanger	$\Delta T_{pinch,gen}$	°C	25
Inlet temperature of preheater (hot side)	T_{17}	°C	25
Outlet temperature of preheater (hot side)	T_{18}	°C	5
Temperature at evaporator outlet	T_{evp}	°C	−5
Temperature at absorber outlet	T_{abs}	°C	30
Temperature at condenser outlet	T_{cond}	°C	30
Effectiveness of solution heat exchanger	ξ	%	90
Heat transfer coefficient of vapor generator, HPHE, LPHE	$U_{heat\ exchanger}$	kW/m^2.K	1.6
Heat transfer coefficient of preheater	$U_{preheater}$	kW/m^2.K	2.0
Heat transfer coefficient of generator	U_{gen}	kW/m^2.K	1.3
Heat transfer coefficient of ARSHE	U_{ARSHE}	kW/m^2.K	0.5
Heat transfer coefficient of evaporator	U_{evp}	kW/m^2.K	1.1
Heat transfer coefficient of absorber	U_{abs}	kW/m^2.K	0.8
Heat transfer coefficient of solution heat exchanger	U_{SHX}	kW/m^2.K	0.7
Logarithmic mean temperature difference at generator	$\Delta T_{gen,LMTD}$	°C	6.28
Logarithmic mean temperature difference at evaporator	$\Delta T_{evp,LMTD}$	°C	13
Logarithmic mean temperature difference at absorber	$\Delta T_{abs,LMTD}$	°C	10
Interest rate	i_r	–	0.12
Operation and maintenance factor	γ	–	1.06
Lifetime of system	n	years	20
Annual operation time of the system	τ	hours	8000

used as the default ORC condenser pressure. Pentane, R123, and cyclopentane are observed to operate with the default values. R123 shows a slightly better performance than pentane, and cyclopentane is observed to have the highest performance among the working fluids being studied, with a second law efficiency of 29.06 % and a net power output of 12,270 kW. This may be because, as the pressure drop during the expansion process for cyclopentane is the highest, and this is observed from the sensitivity analysis shown in the subsequent section of the paper, the work output from the expansion process was higher than the work input from pumping a fluid to a higher pressure. In that context, ethylbenzene is supposed to have the worst performance as it has the smallest pressure difference between the turbine and condenser. However, ethylene showed the lowest performance in terms of second law efficiency (13.99 %) and net work output (6693 kW). While ethylene has the 3rd smallest pressure difference, the main reason why ethylene showed an even worse performance is because it is a wet fluid (i.e., saturated vapor line has a negative slope in T-s diagram).

A higher percentage of liquid during the expansion process can be detrimental to the turbine blades as it may cause cavitation. Therefore, the use of ethylene is not recommended unless a high degree of superheating can be provided. The degree of superheating is reduced for R245fa as the temperature at the turbine inlet exceeds its operable range. The same reduction is applied isobutane, where a temperature difference of 28.1 °C results in a negative exergy destruction rate in the component, HPHE, indicating system failure. For ethylene and toluene to be utilized as working fluids, the condenser pressure of ethylene must increase substantially, whereas it should slightly decrease for toluene. This is necessary for ethylene as the default condenser pressure lowers the temperature of carbon dioxide in the TCO_2 cycle below its workable range. For toluene, reducing both the turbine inlet and condenser pressure ensures that there is no heat transfer from the ORC to the vapor generator at the default degree of superheating. Given that the model is validated based on the cascade ORC-TCO_2-LNG cycle proposed by Sadreddini et al. [5], the proposed ACPLU aims to achieve two criteria: (1) A second law efficiency higher than 13.1 % and (2) A net work output above 8.12 MW. All working fluids, except for ethylene is observed to satisfy these criteria.

Fig. 5. Framework for mathematical modelling of the proposed CCP system.

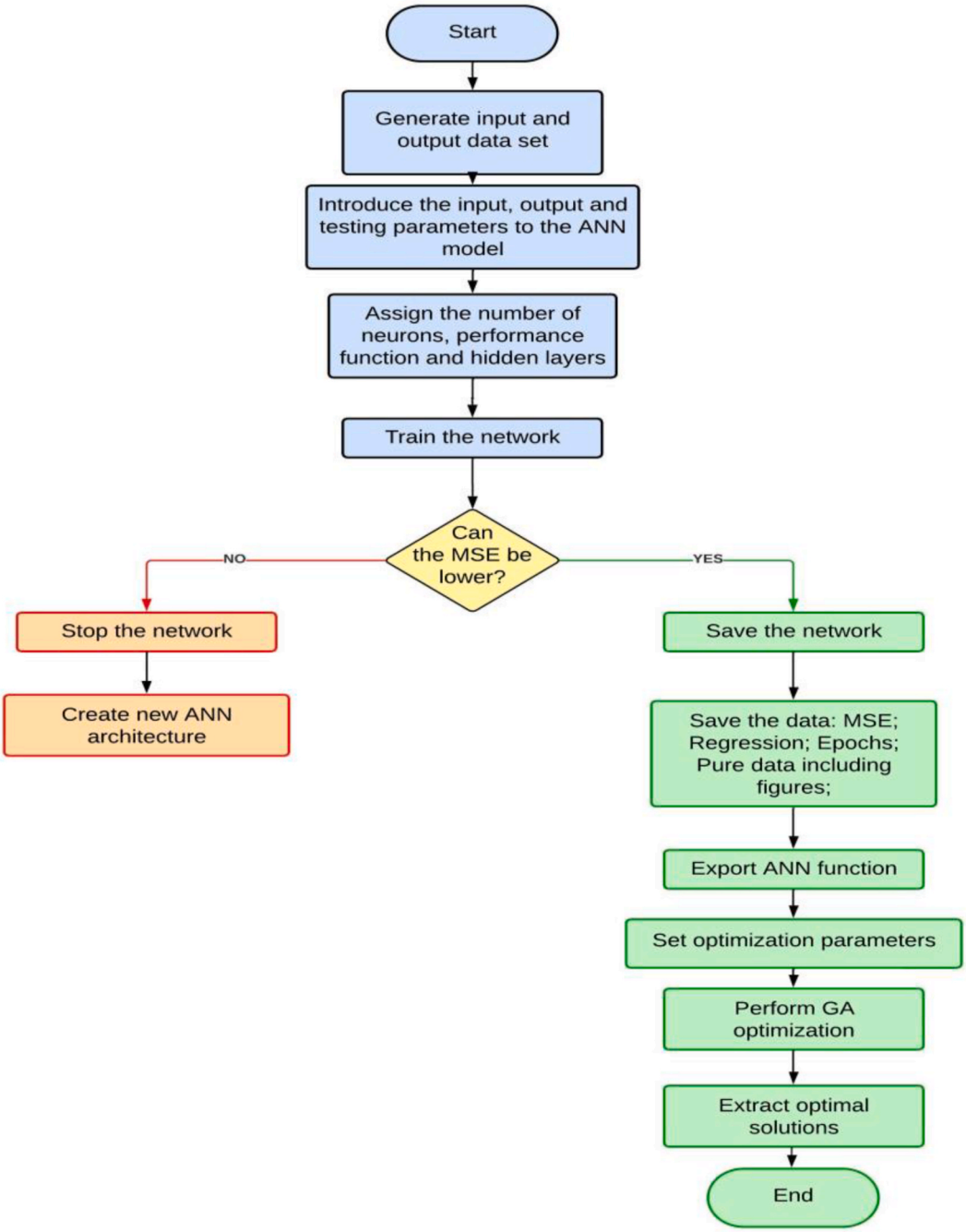

Fig. 6. Mult-objective optimization flow chart.

8.2. Sensitivity analysis

Utilizing the boundary conditions shown in Table 15, the effect of the various parameters on the mass flow rate, work output on each cycle, net work output and second law efficiency were examined. The boundary conditions for the power cycle were sourced from a previous study [5]. To ensure consistency with the previous study, pentane was chosen as the ORC working fluid. Given that the heat exchanger, ARSHE, and generator play crucial roles in integrating the power cycle with the ARS, greater emphasis must be given on validating this integration. Hence, a sensitivity analysis on the effect of pinch temperatures of ARSHE and the generator was conducted. Additionally, the influence of evaporator temperature on the overall performance of the ACPLU was bjstudied.

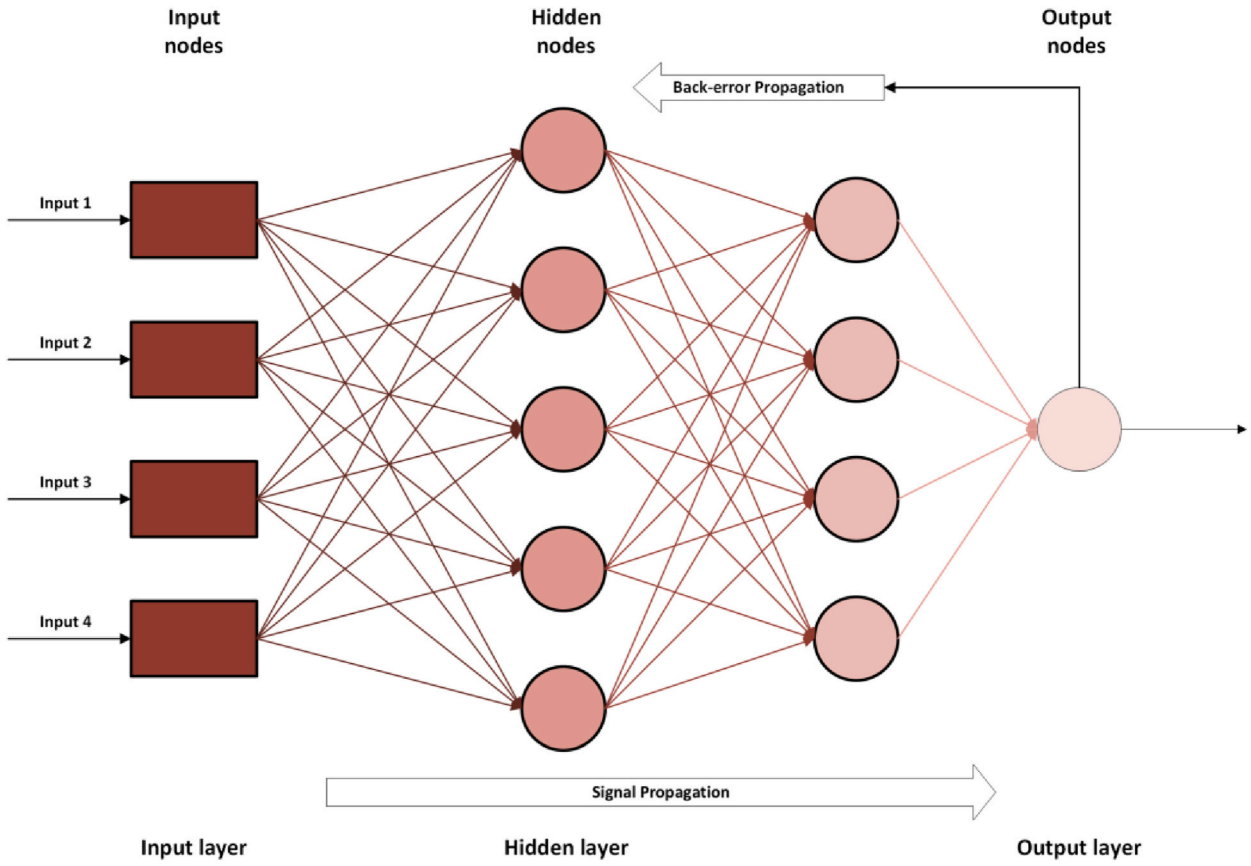

Fig. 7. Illustration of an ANN model with back-propagation.

Table 9
Constraints used in the GA algorithm to conduct the MOO.

Parameters	Unit	Lower limit	Upper limit
Heat source temperature	°C	250	450
CO_2 condenser pressure	bar	6	14
ARSHE pinch	°C	8	63

Table 10
Operating parameters used in the GA.

Parameters	Value
Population size	200
Crossover function	singlepointcrossover
Mutation function	mutationadaptfeasible

8.2.1. Effect of heat source temperature

Fig. 9(a) illustrates that an increase in heat source temperature results in more heat being absorbed by the vapor generator. Consequently, this increases the temperature of the working fluid, enabling higher mass flow rates in each cycle. This increase in mass flow rate means more superheated fluid enters the turbines, resulting in greater power generation.

In Fig. 9(b), the net work of the system increases rapidly with higher heat source temperature. However, despite the anticipated trend of an increasing second law efficiency with rising heat source temperature, the second law efficiency for the ACPLU decreased exponentially. This is attributed, and later proved in the subsequent exergy analysis section, to the increasing average temperature between the inlet and outlet of the heat source, which increases the net rate of exergy destruction of the ACPLU system. While the total useful work output does increase with higher heat source temperature, it does so in a slower rate, resulting in an overall decrease in second law efficiency.

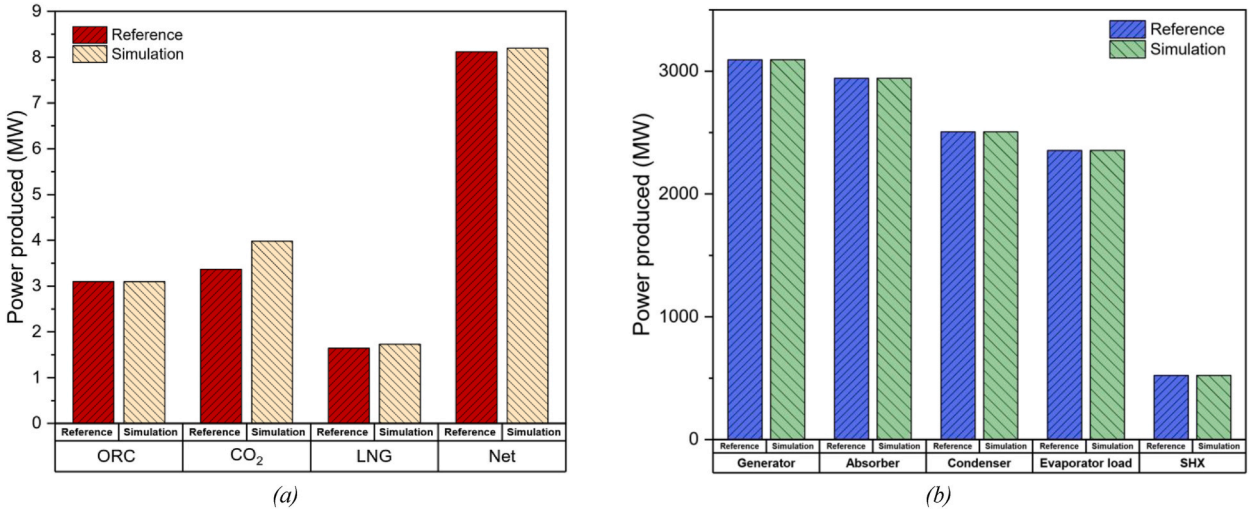

Fig. 8. Bar charts comparing important parameters of reference values and calculated values of: (a) Power cycle and (b) Absorption refrigeration system.

Table 11
Comparison of the calculated value and the reference values for the ORC-TCO_2-LNG system and ARS.

Cascaded ORC-TCO_2-LNG cycle				ARS			
Parameters	Reference value [5]	Calculated value	Error (%)	Parameters	Reference value [56]	Calculated value	Error (%)
Power produced by ORC, $\dot{W}_{ORC}$ (kW)	3.10	3.098	0.07	Generator input, $\dot{Q}_{gen}$ (kW)	3093	3094	0.03
Power produced by TCO_2 cycle, $\dot{W}_{CO_2}$ (kW)	3.37	3.398	0.20	Absorber heat rejected, $\dot{Q}_{abs}$ (kW)	2943	2943	0
Power produced by LNG cycle, $\dot{W}_{LNG}$ (kW)	1.65	1.730	4.85	Condenser heat rejected, $\dot{Q}_{cond}$ (kW)	2506	2506	0
Power output, $\dot{W}_{net}$ (kW)	8.12	8.196	0.94	Evaporator load, $\dot{Q}_{evp}$ (kW)	2355	2356	0.03
				Heat rejected by hot side of solution heat exchanger, $\dot{Q}_{SHX}$ (kW)	522.6	522.9	0.57
				COP	0.7615	0.7615	0

8.2.2. *Effect of superheating*

Degree of superheating describes the extent to which a fluid is superheated. Fig. 10(a) shows that, with an increase in the degree of superheating, the work output from the TCO_2 cycle increases, but decreases for the LNG cycle. The work done for the ORC increases slightly till 5 °C and then decreases linearly, therefore showing an optimum value of 4233 kW at 5 °C. As both the ORC and LNG cycle exhibit a decrease in their power production rate with an increase in degree of superheating, the rate of increase in power produced by the TCO_2 must offset it for an overall positive net work output. In the case of mass flow rates, all three cycles show a general decrease in mass flow rates.

Fig. 10(b) illustrates the net work output increases slightly with rising degree of superheating (5.4 % increase when degree of superheating is increased by 50 °C), were the net power output for the TCO_2 cycle is the most sensitive to the degree of superheating. Simultaneously, the second law efficiency also increases significantly (from 25.92 % to 27.77 %). This may be attributed to the greater utilization of heat from the heat source. It can be concluded that increasing the degree of superheating will have little significance in improving the net work output of the proposed cycle but will contribute substantially in increasing the second law efficiency.

8.2.3. *Effect of condenser pressure (lower pressure)*

Variation in condenser pressure can alter the saturation temperature of the ORC's working fluid and impact the pressure ratio of the ORC turbine, resulting in a notable effect in performance. As shown in Fig. 11(a), increasing ORC condenser pressure leads to a significant decrease in the work done by the ORC, despite the slight rise in the ORC's mass flow rate. This is primarily attributed to the low-pressure ratio in the ORC turbine, which reduces its work output. However, both the TCO_2 and LNG cycle has a slight increase in work output, which is evident by the rising mass flow rates in these cycles.

Since the sensitivity of the ORC's work done to the ORC condenser pressure is more pronounced relative to the TCO_2 and LNG cycle, the net work done by the ACPLU decreases with increase in ORC condenser pressure, as shown in Fig. 11(b). With the decrease in net work output, the second law efficiency also declines. This is evident because a lower pressure ratio leads to a lower expansion process.

Table 12
Computed results of combined power (Pentane-TCO_2) and refrigeration cycle (LiBr–H_2O).

State	Temperature, T (°C)	Pressure, P (bar)	Enthalpy, h (kJ/K)	Entropy, s (kJ/kg-K)	Mass flow rate, ṁ (kg/s)
0	25	1.013	577.1	7.521	–
1	300	1.013	579.2	7.525	120
2	100	1.013	374.1	7.085	120
3	47.2	1.465	27.2	0.086	37.91
4	49.12	33	34.2	0.092	37.91
5	195.2	33	490.7	1.234	37.91
6	195.2	33	548.1	1.357	37.91
7	223.3	33	683.3	1.639	37.91
8	141.6	1.465	565.1	1.690	37.91
9	133.6	80.13	562.2	2.114	43.67
10	−32.68	6	450.2	2.200	43.67
11	−53.12	6	86.8	0.552	43.67
12	−49.81	80.13	95.2	0.561	43.67
13	−161.7	1.013	−0.8	−0.007	77.73
14	−158.4	70	20.9	0.041	77.73
15	−103.1	70	225.1	1.484	77.73
16	−25	70	691.8	3.759	77.73
17	5	1.013	21.1	0.076	432.9
18	25	1.013	104.9	0.367	432.9
19	25	70	840	4.305	77.73
20	−11.22	40	779.5	4.346	77.73
21	60	1.013	333.6	6.970	120
22	75	0.0425	2640.0	8.713	1
23	30	0.0425	125.7	0.437	1
24	−5	0.00402	125.7	0.492	1
25	−5	0.00402	2491	9.314	1
26	30	0.00402	93.0	0.1643	35.56
27	30	0.0425	93.0	0.1643	35.56
28	71.3	0.0425	167.2	0.4111	35.56
29	75	0.0425	188.1	0.421	34.56
30	34.5	0.00431	111.7	0.1875	34.56
31	34.5	0.00431	111.7	0.1875	34.56

Table 13
Fluid properties of carbon dioxide, methane and tested organic fluids [5,68–74].

Working fluid	T_{crit} (°C)	P_{crit} (bar)	Type of fluid	Triple point (°C)	Maximum allowable temperature (°C)	Normal boiling point (°C)
Carbon dioxide	30.98	73.77	Wet	−56.41	1726.9	−78.4
Methane	−82.586	45.99	Wet	−182.46	351.85	−161.7
Pentane	196.55	33.7	Dry	−129.68	326.85	36.06
R123	183.68	36.72	Dry	−107.15	326.85	27.82
Isobutane	134.66	32.29	Dry	−159.42	301.85	−11.75
R24fa	153.86	36.51	Dry	−102.1	166.85	15.30
Cyclopentane	238.57	45.71	Dry	−93.45	276.85	49.2
Ethylene	9.20	50.42	Wet	−169.16	176.85	−103.7
Ethylbenzene	343.97	36.22	Dry	−94.95	426.85	136
Toluene	318.60	41.26	Dry	−95.15	426.85	110.6

Table 14
Computed performance parameters of the ACPLU with different working fluids.

Working fluids	Net work (kW)	1st law efficiency (%)	2nd law efficiency (%)	Maximum temperature for superheating (°C)	ORC turbine inlet pressure range (bar)	ORC condenser pressure (bar)
Pentane	11761	39.91	27.3	28.1	33	1.4653
R123	11807	40.06	27.45	28.1	36	1.4653
Cyclopentane	12270	41.63	29.06	28.1	45	1.4653
Ethylbenzene	10237	34.74	22.57	28.1	3	1.4653
Ethylene	6693	22.71	13.99	28.1	50	25
R245fa	11310	38.38	25.82	13.5	36	1.4653
Isobutane	11071	37.57	25.06	12.7	32	1.4653
Toluene	11801	27.43	28.68	28.1	10	0.6

Table 15
Boundary Conditions used for sensitivity analysis.

Input Variable	Unit	Lower limit	Upper limit	Optimum value
Heat source temperature	°C	250	450	300
ΔT_{sup}	°C	0	50	28.1
Turbine inlet pressure of ORC	bar	16	33	33
Condenser pressure of ORC	bar	1	4	1.4653
Turbine inlet pressure of TCO_2 cycle	bar	72	90	80.13
Condenser pressure of TCO_2 cycle	bar	6	14	6
Pinch (HPHE)	°C	8	17	8
Pinch (LPHE)	°C	15	60	50
Pinch (ARSHE)	°C	8	63	50
Pinch (Generator)	°C	10	25	25
Evaporator temperature	°C	−5	0	−5

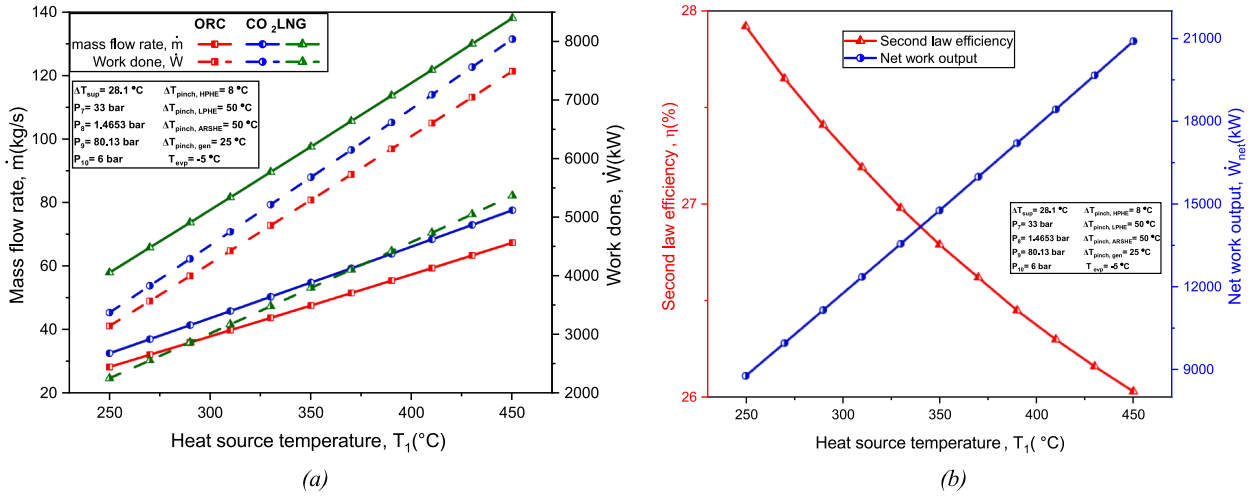

Fig. 9. Effect of heat source temperature on: (a) Mass flow rate and work done of each cycle; (b) Second law efficiency and net work done.

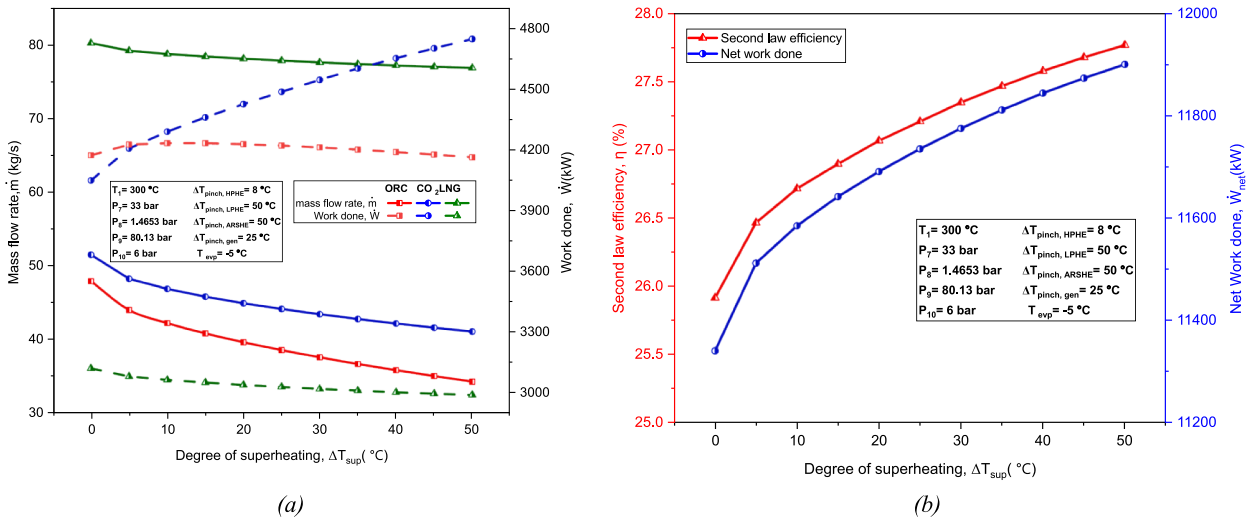

Fig. 10. Effect of degree of superheating on: (a) Mass flow rate and work done of each cycle; (b) Second law efficiency and net work.

This observation leads to the conclusion that ORC condenser pressure significantly affects the work output of the ORC.

By examining the effect of CO_2 condenser on mass flow rate and work done by each cycle, Fig. 12(a) reveals a decrease in work done for both the TCO_2 and LNG cycle. For the LNG cycle, this decrease is accompanied by a corresponding drop in the mass flow rate.

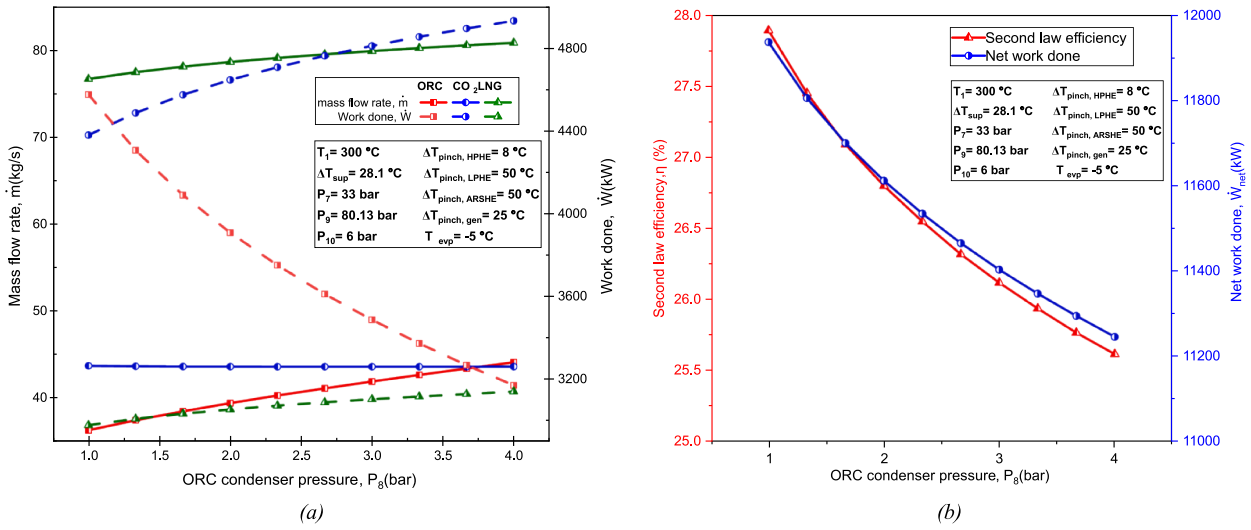

Fig. 11. Effect of ORC condenser pressure: (a) Mass flow rate and work done of each cycle; (b) Second law efficiency and net work done.

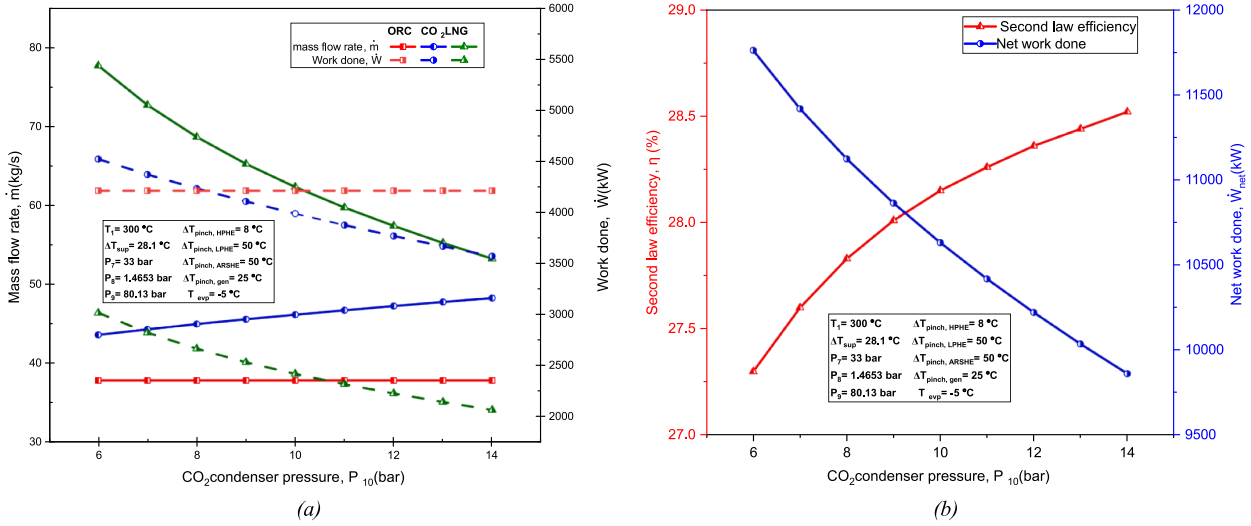

Fig. 12. Effect of CO_2 condenser pressure: (a) Mass flow rate and work done of each cycle; (b) Second law efficiency and net work done.

However, the mass flow rate of the TCO_2 cycle increases slightly. Therefore, the reduction in work output for the TCO_2 cycle may be attributed to a similar cause as the decrease in work output for the ORC, namely, the lower pressure ratio in the TCO_2 cycle resulting from an increase in TCO_2 cycle condenser pressure.

With respect to net work done, varying CO_2 condenser pressure results in a trend similar to that of varying condenser pressure for ORC, as shown in Fig. 12(b). As the condenser pressure for TCO_2 increases, the net work done decreases. In contrast to the decrease in second law efficiency observed with an increase in ORC condenser pressure, an increase in CO_2 condenser pressure leads to a significant improvement in second law efficiency. This could be attributed to the decreased temperature difference between LPHE's hot and cold side. Compared to the proportional relationship between overall net work output and second law efficiency in the ORC, the inverse relationship in the TCO_2 cycle elucidates that a smaller temperature difference between the hot and cold side of LPHE has a greater positive effect on second law efficiency than the negative effect from the reduced pressure ratio. This is further explored and explained in the subsequent sections.

8.2.4. Effect of turbine inlet pressure (upper pressure)

Fig. 13(a) depicts that; mass flow rate decreases across all cycles. Altering ORC turbine inlet pressure increases the ORC work done significantly, while the LNG and TCO_2 cycle experiences a slight decrease. Similar to the case of increasing condenser pressure, the increase in ORC work output is more sensitive compared to the decrease in TCO_2 and LNG work output, with rising ORC turbine inlet pressure. The increase in ORC work output is likely a result of the higher-pressure ratio stemming from the higher turbine inlet

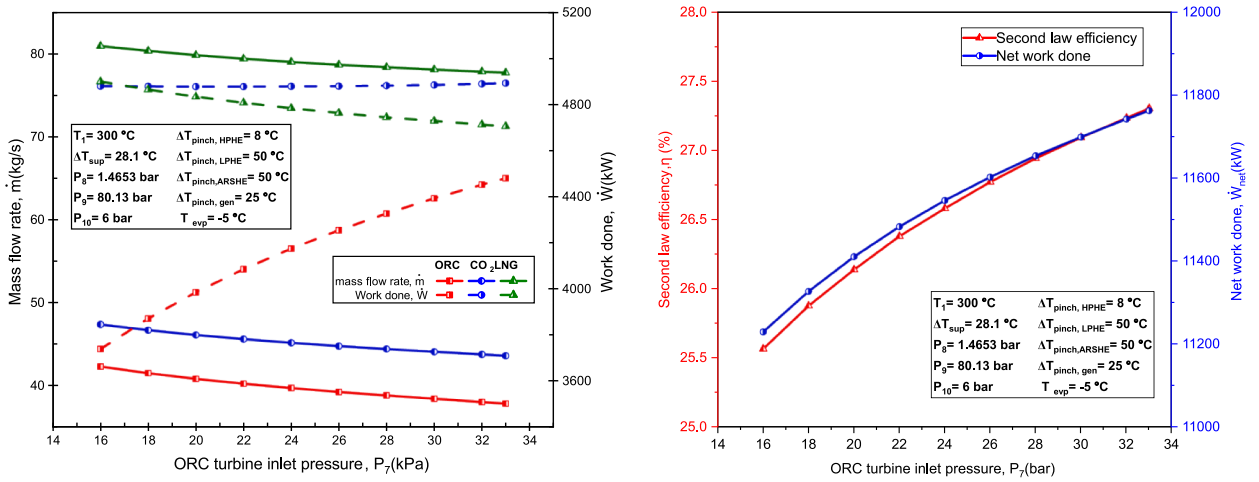

Fig. 13. Effect of ORC turbine inlet pressure on: (a) Mass flow rate and work done of each cycle; (b) Second law efficiency and net work done.

pressure. Hence, the net work done increases significantly with rising ORC turbine inlet pressure, as illustrated in Fig. 13(b). Consequently, the second law efficiency also increases as more useful energy is utilized.

For the TCO_2 cycle to operate in transcritical conditions, the turbine inlet pressure must exceed the CO_2 critical pressure (73.77 bar) while the condenser pressure must remain below it. As depicted in Fig. 14(a), the mass flow rate of the ORC remains constant with varying CO_2 turbine inlet pressure, resulting in the ORC's constant work output. The mass flow rate, and consequently, the work output from the TCO_2 increases very slightly as turbine inlet pressure increases. Conversely, there is a slight decrease in the mass flow rate with increasing CO_2 turbine inlet pressure, resulting in a slight decreased work output in the LNG cycle. By combining all individual work outputs, it can be observed in Fig. 14(b), that the net work done increases slightly with the increase in the TCO_2 turbine inlet pressure. Due to the development of the extra net work output, the second law efficiency also increases slightly.

8.2.5. Effect of pinch on system performance

Fig. 15 illustrates the effect of the high-pressure heat exchanger, HPHE pinch temperature in system performance. The mass flow rate and work done by the ORC and LNG cycle remains relatively constant with increasing pinch temperature, as shown in Fig. 15(a). The mass flow rate of the TCO_2 cycle increases slightly while the work output slightly decreases. This is attributed to the turbine's decreasing work output with increasing pinch temperature. In Fig. 15(b), at lower pinch temperatures, the system performs better. This may be due to less exergy destruction at lower pinch.

In Fig. 16, variation in the low-pressure heat exchanger, LPHE, pinch temperature can significantly affect the ACPLU system

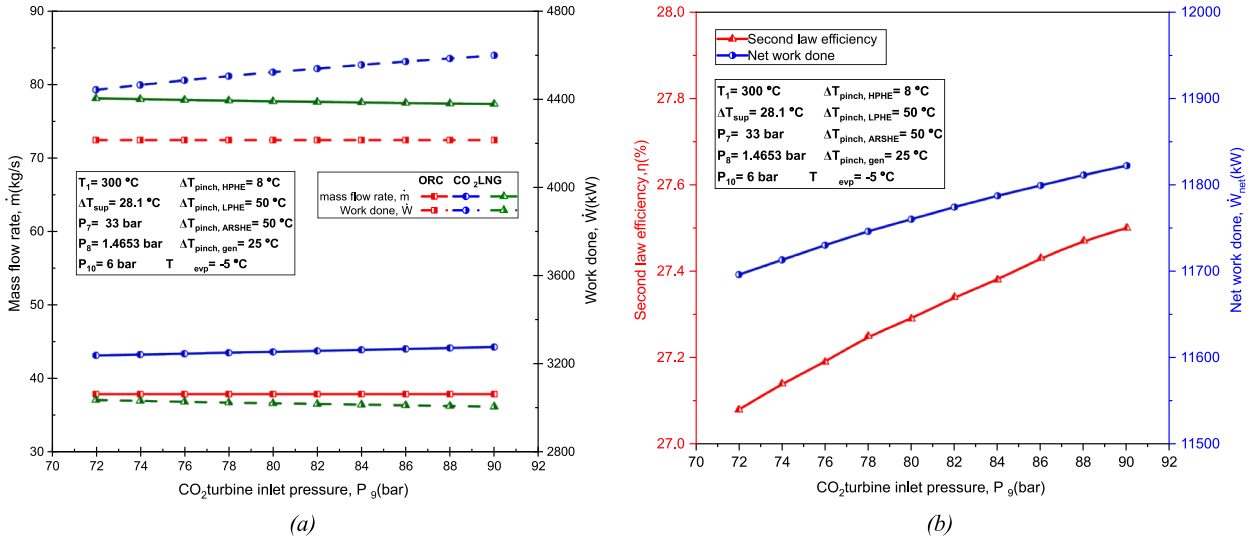

Fig. 14. Effect of CO_2 turbine inlet pressure on: (a) Mass flow rate and work done of each cycle; (b) Second law efficiency and net work done.

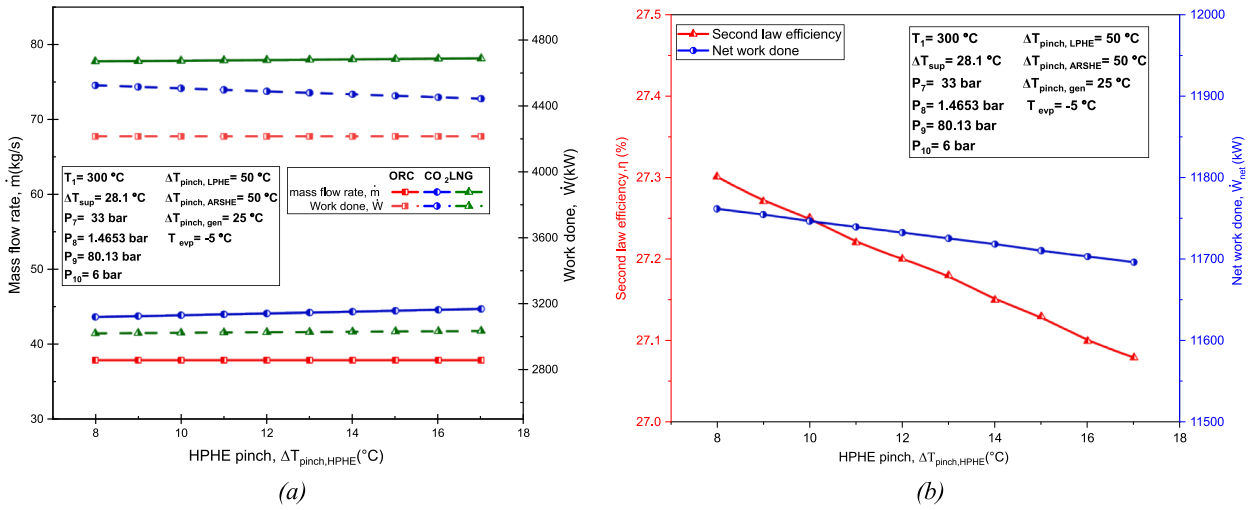

Fig. 15. Effect of HPHE pinch temperature on: (a) Mass flow rate and work done of each cycle; (b) Second law efficiency and net work done.

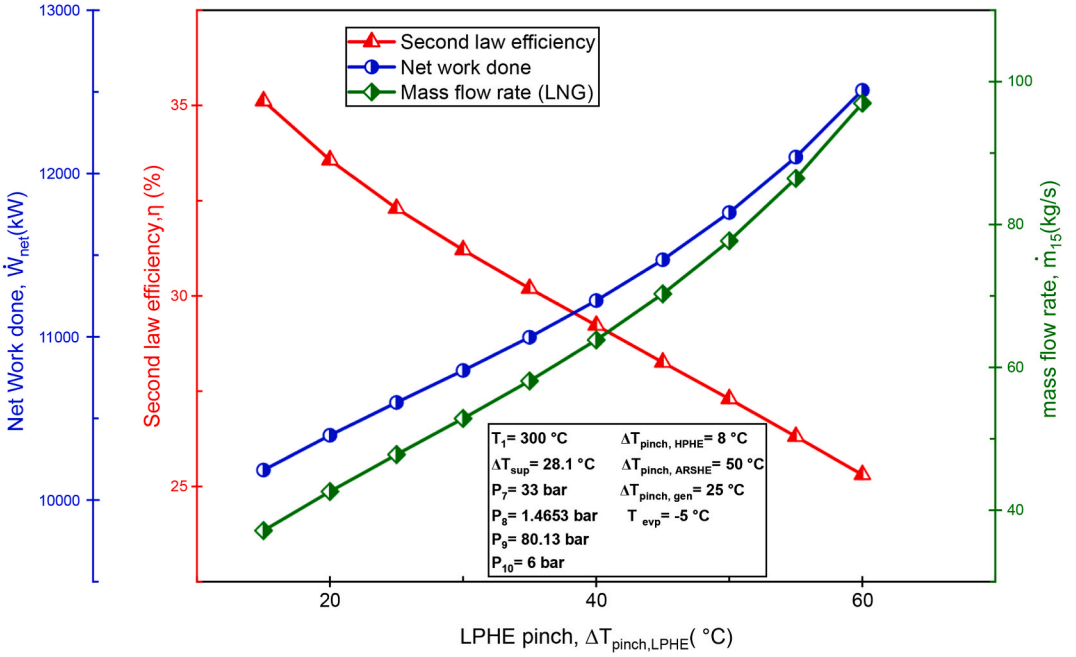

Fig. 16. Effect of LPHE pinch temperature on system performance.

performance. With increasing LPHE pinch temperatures, the LNG stream mass flow rate also increases. The increased mass flow rate elucidates the increased net work done. However, simultaneously, it leads to a decrease in second law efficiency. From this analysis, it can be concluded that a lower pinch temperature is recommended if the aim is to develop a more efficient CCP system utilizing LNG cold energy.

Cold energy from the LNG cycle is still available that can be used as a heat sink. Hence, integrating the ARSHE between the LNG and ARS cycle results in the general increase in LNG working fluid temperature (in state 19 of Fig. 3), resulting in a higher turbine work output. Shown in Fig. 17, the net work output and second law efficiency increases with increasing ARSHE pinch temperature. Similar to the heat exchanger, LPHE, increasing ARSHE pinch does not increase the overall exergy input rate while increasing the heat absorbed by the LNG stream, resulting in the increased system performance.

8.2.6. Effect of ARS parameters on system performance

Studies have shown that variations in evaporator temperature, T_{evp} significantly affect the system performance of the ARS [75]. Since the generator pinch temperature, $\Delta T_{pinch,gen}$, is also a crucial operating parameter, a dual parametric analysis of the ACPLU

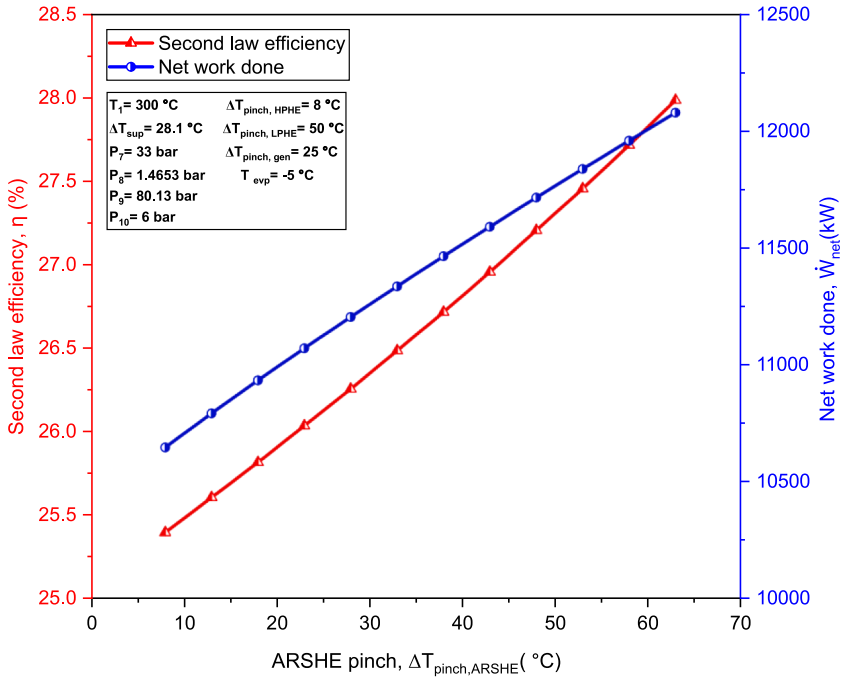

Fig. 17. Effect of ARSHE pinch temperature on system performance.

system is conducted. As shown in Fig. 18(a), increasing generator and evaporator temperature improves the COP. This may be due to the higher heat absorption rate from the heat source. The generator pinch temperature does not have any effect on the second law efficiency and heat absorbed by the evaporator, while increasing evaporator temperature makes the second law efficiency suffer and increases the heat absorbed by the evaporator, as shown in Fig. 18(b) and (d) respectively. This may be due to the higher heat absorbed by the water from the concentrated LiBr solution inside the absorber. As shown in Fig. 18(c), temperature variations in the generator and evaporator does not have any effect on net work done by the ACPLU system, as the ARS is not responsible for power production and the power needed in the pumping process in the ARS is negligible.

8.3. *Exergy analysis of the proposed ACPLU system*

The flow of exergy rate of the ACPLU system and system components' exergy destruction rate is depicted in Fig. 19. The negligible exergy destruction in the solution pump and expanders, is disregarded and put together as one outflow. The most significant exergy loss is shown to be in the LNG stream, with the maximum being in the preheater and LPHE. This may be due to most of the LNG stream being exhausted out. While the LNG can be used in its re-gasified state, which would facilitate its remaining exergy, it is not in our scope of study and remains a potential research gap to investigate. In the ARS system, it is expected that the solution heat exchanger (SHX) and the generator would be the chief contributors to the exergy destruction rate [76]. The relatively high exergy destruction in the generator (147.1 kW) and SHX (211,2 kW) in the ARS elucidates that. However, the highest exergy destruction rate in the ARS was observed to be in the evaporator (263.3 kW). This may be due to the environmental condition of the proposed system, which was assumed to be room temperature.

A comprehensive parametric analysis on the exergy destruction is shown from Figs. 20–24. As indicated in Fig. 20(a), the overall exergy destruction increases significantly with increase in pinch temperature. This can be elucidated further by understanding that the amount of heat wasted in the atmosphere is more when any of the system components transfers heat to the dead state, even if the net work done increases with rising heat source temperature. Furthermore, it is harder to maintain heat exchanger effectiveness at higher temperature, as shown by the increased exergy destruction in the preheater and LPHE. Due to the higher heat utilization of the waste heat source, the overall exergy destruction decreases with increasing degree of superheating, as shown in Fig. 20(b). Therefore, less heat is wasted to the surrounding. Evidently, the most significant decrease in exergy destruction of the component with increase in degree of superheating was in the vapor generator.

Fig. 21(a) illustrates that, there is a slight decrease in exergy destruction with rising ORC turbine inlet pressure. At higher pressures, the utilization of heat from the heat source is enhanced [58]. This is elucidated by the significant decrease in the vapor generator exergy destruction rate. Conversely, Fig. 21(b), depicts an inverse trend with increasing ORC condenser pressure. While the vapor generator and ORC turbine exergy destruction rate decreases, it increases in all the other components of the power cycle, especially in the HPHE. This suggests that, increasing the ORC condenser pressure results in a lower pressure ratio in the cascaded cycle, resulting in more exergy being wasted, which may be due to the weakened heat transfer rate in the heat exchanger. Fig. 21(c) follows a similar

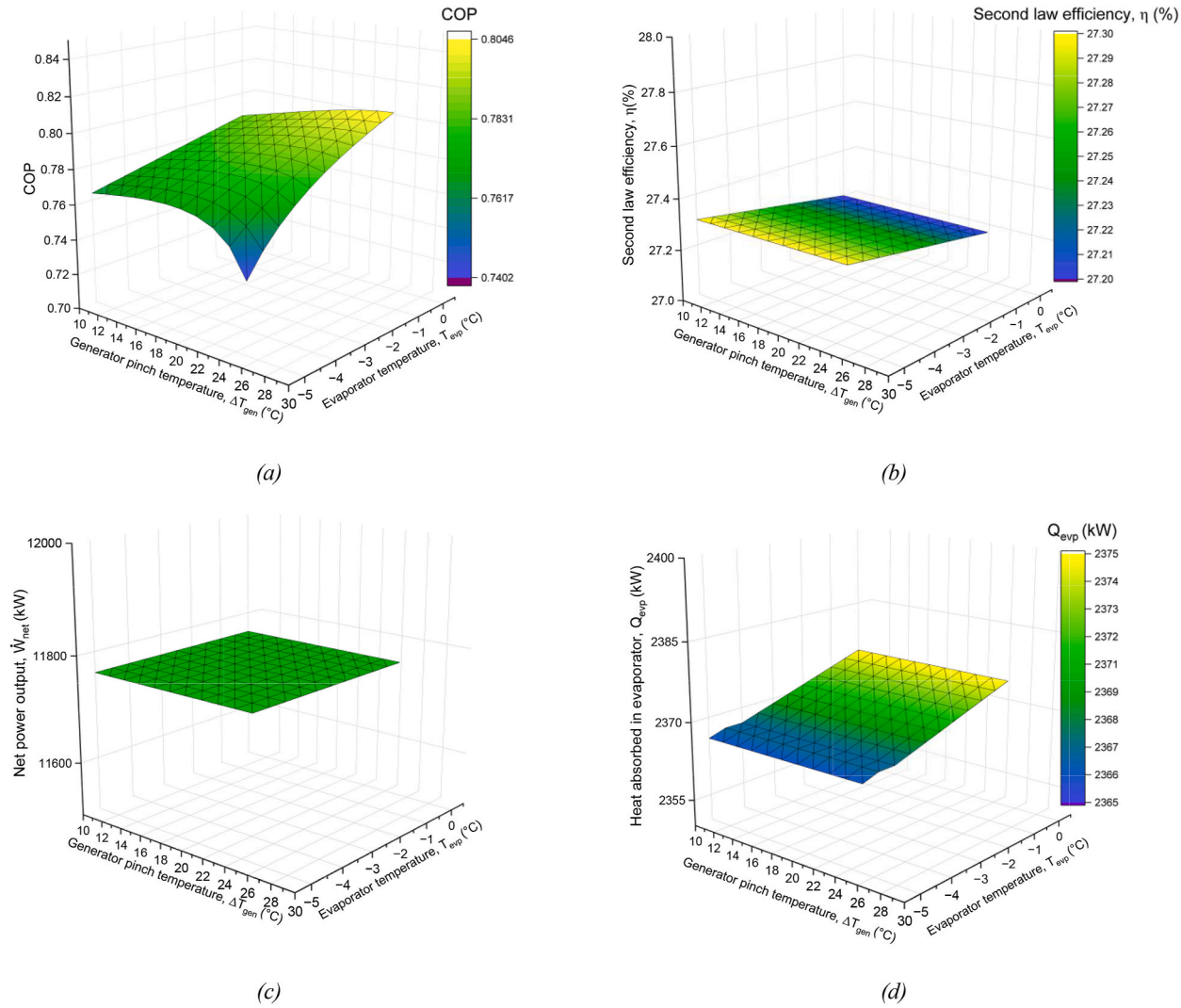

Fig. 18. Effect of generator pinch and evaporator temperature on: (a) COP (Coefficient of performance); (b) Second law efficiency; (c) Net work done; (d) Heat absorbed by evaporator.

trend to Fig. 21(a), albeit to a negligible extent. However, the increase in CO_2 condenser pressure produces a significant reduction in overall exergy destruction, as illustrated in Fig. 21(d), due to the decrease in exergy destruction rate of both the HPHE and preheater. This may be attributed to the rise in LPHE hot side inlet temperature, which raises the LNG stream overall temperature, reducing the preheater's temperature difference between it's hot and cold side and, consequently, reducing its exergy destruction.

As depicted in Fig. 22(a) and (b), while increasing the generator temperature and evaporator reduces the generator's and absorber's exergy destruction rate as more heat is utilized from the waste heat source, the reduction is negligible relative to overall exergy destruction rate. Hence, the overall exergy destruction remains almost constant.

Although the higher HPHE pinch temperature makes the exergy destruction rate of the HPHE and LPHE increase due to the larger temperature difference between the heat exchanger's hot and cold side, the increase is very negligible relative to overall exergy destruction rate, as shown in Fig. 23(a). However, in Fig. 23(b), the rising LPHE pinch temperature increases the exergy destruction rate of the LPHE significantly. As the average temperature of the LNG stream is dependent on the pinch temperature of the LPHE, the temperature difference in the preheater increases significantly, resulting in the large rate of exergy destruction. In conclusion, the overall exergy destruction rate exhibits an almost linear increase with increasing pinch temperature Therefore, a lower pinch temperature in the LPHE is recommended.

Shown in Fig. 24, the exergy destruction of the ACPLU system increases slightly, reaching a maximum at 38 °C and then decreasing slightly, with increase in ARSHE pinch temperature. Beyond 38 °C, the rising exergy destruction rate of the evaporator, expansion valves and SHX is outweighed by destruction rate fall in the generator and absorber, resulting in a slightly decreasing overall exergy destruction.

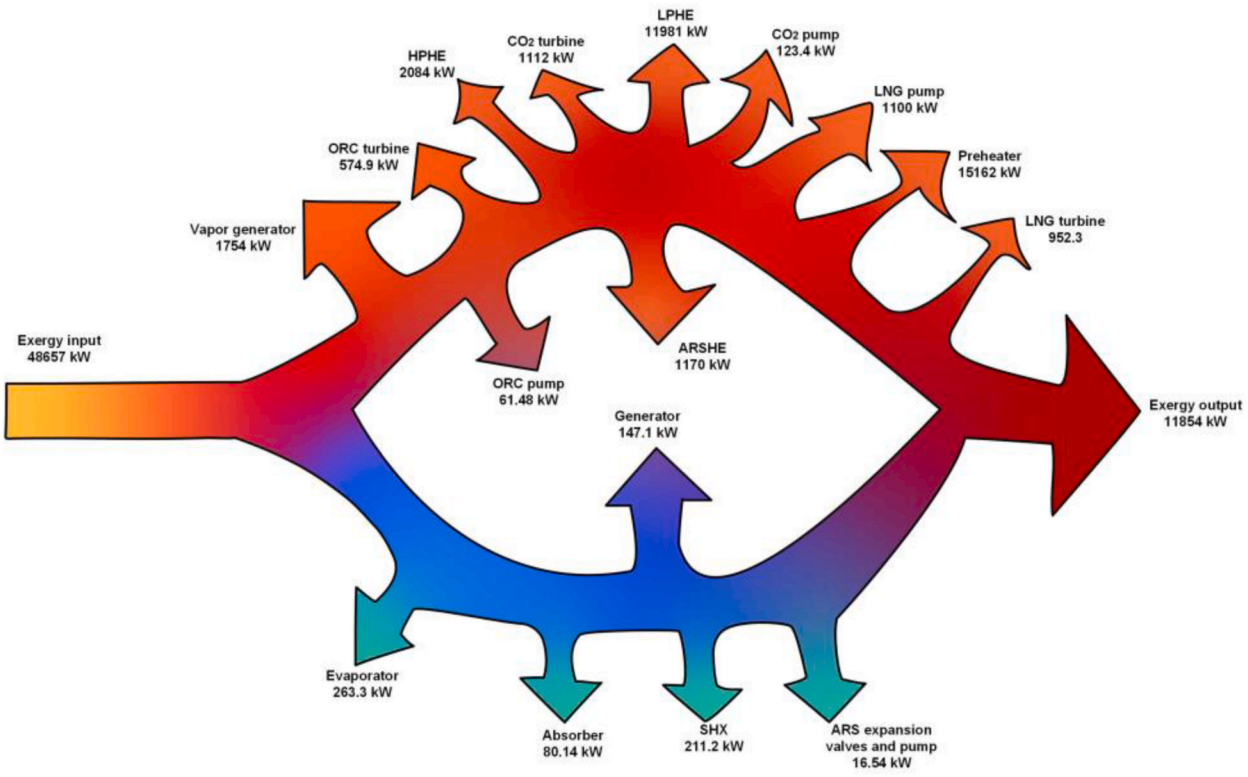

Fig. 19. *Flow diagram of exergy destruction for each component in the ACPLU system.*

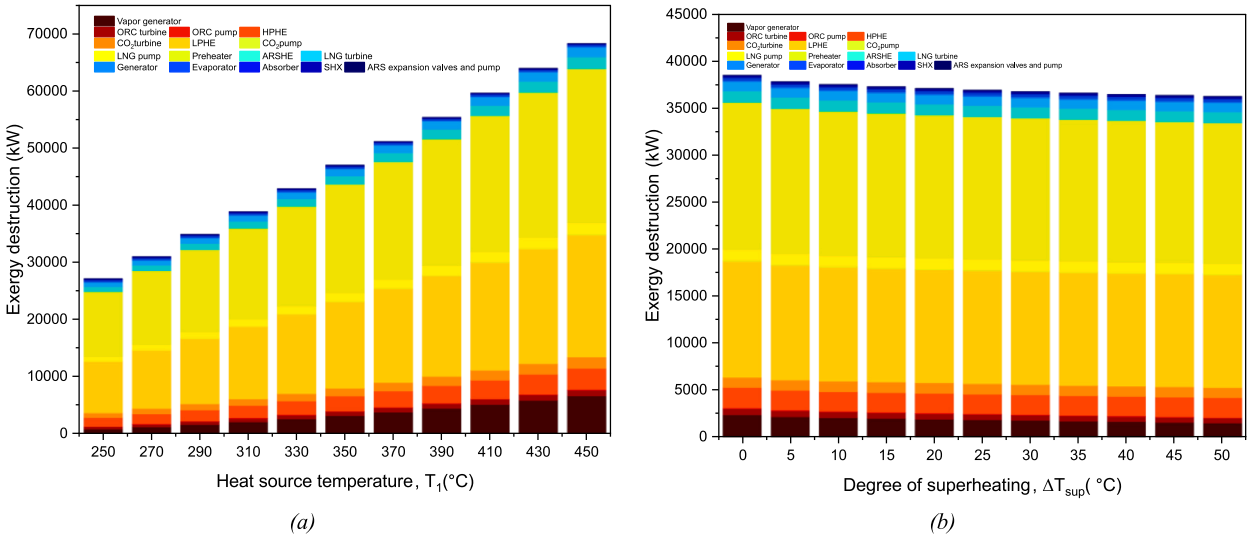

Fig. 20. Effect of exergy destruction with: (a) Heat source temperature. (b) Degree of superheating.

8.4. Thermo-economic performance of the proposed ACPLU system

The economic performance of the ACPLU system, in terms of cost rate, is shown in Table 16. The cost rate of the ARS pump was negligible compared to the cost rate of the rest of the components, hence it was omitted. It can be observed that, among heat exchangers, the cost rate of the preheater is the highest, at 3.263 $/h followed by HPHE, SHX, LPHE, and ARSHE at 1.526 $/h, 1.308 $/h, 0.805 $/h, and 0.224 $/h respectively. The relatively high cost rate of the preheater may be attributed to the relatively low temperature difference between the hot and cold side. Implementing an additional preheater or putting the ARSHE before the preheater

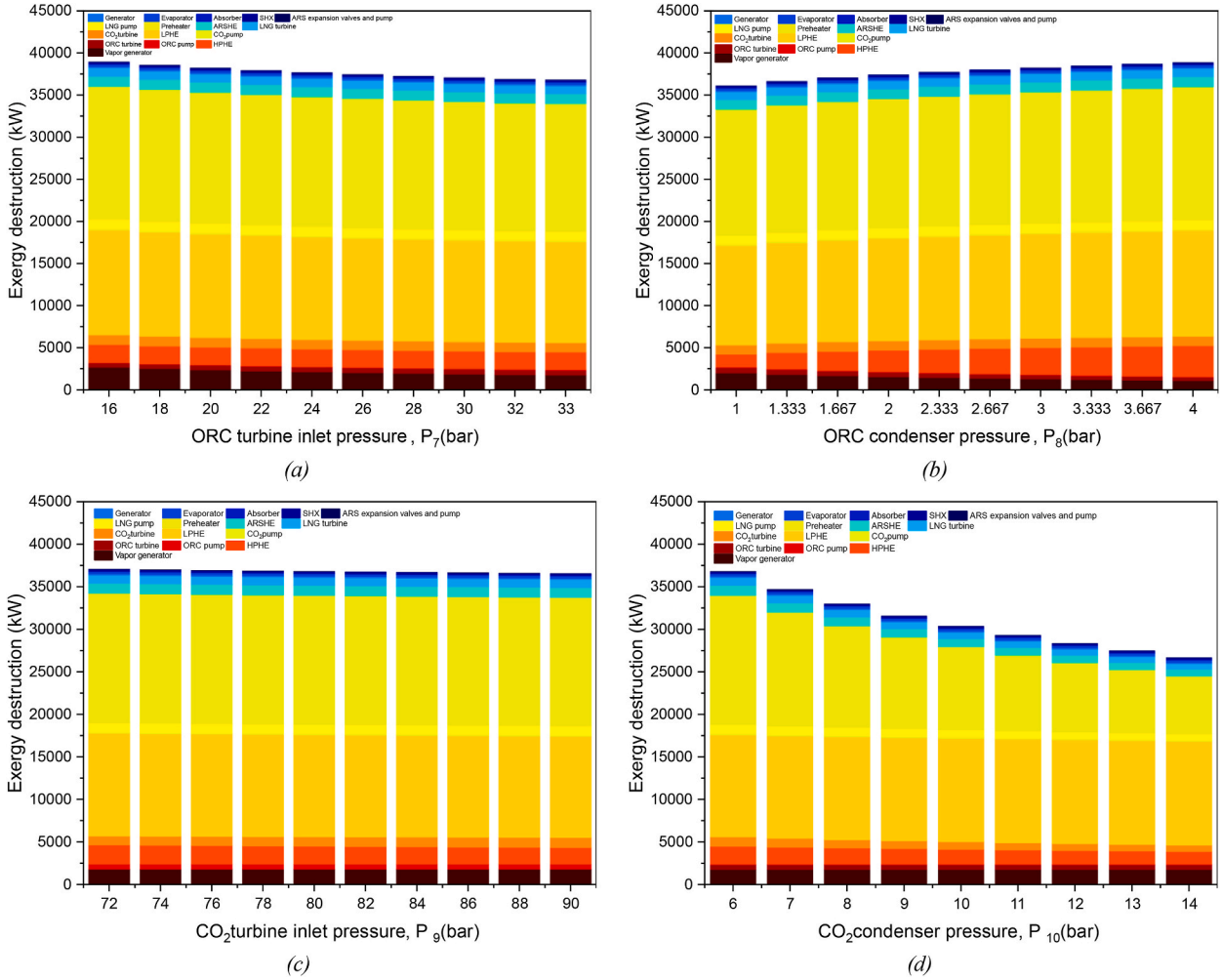

Fig. 21. Effect of exergy destruction with increase in: (a) ORC turbine inlet pressure (b) ORC condenser pressure. (c) CO_2 turbine inlet pressure. (d) CO_2 condenser pressure.

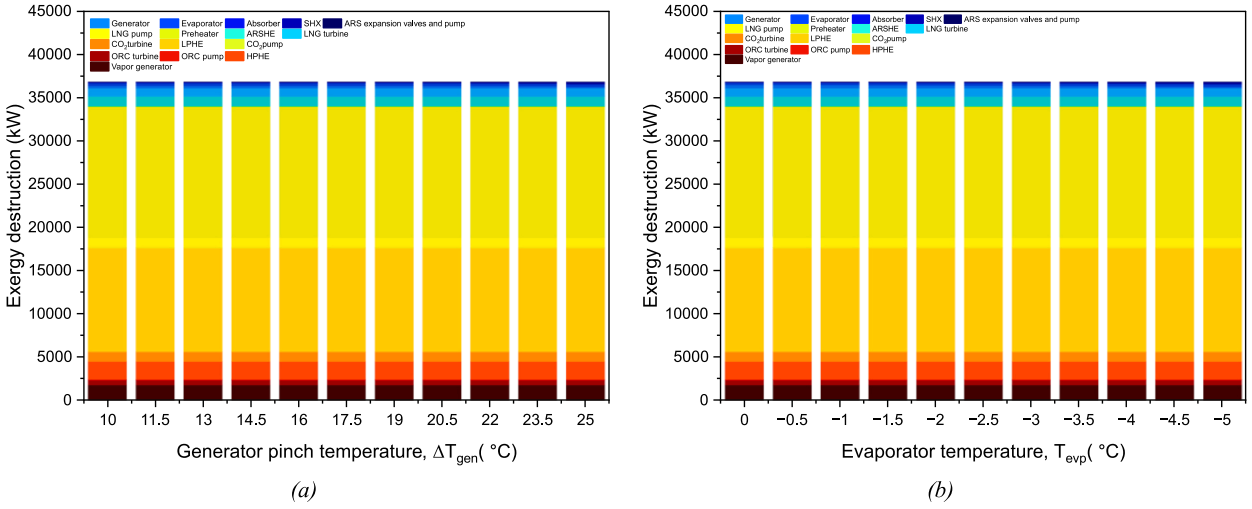

Fig. 22. Effect of exergy destruction with decrease in: (a) Generator pinch temperature. (b) Evaporator temperature.

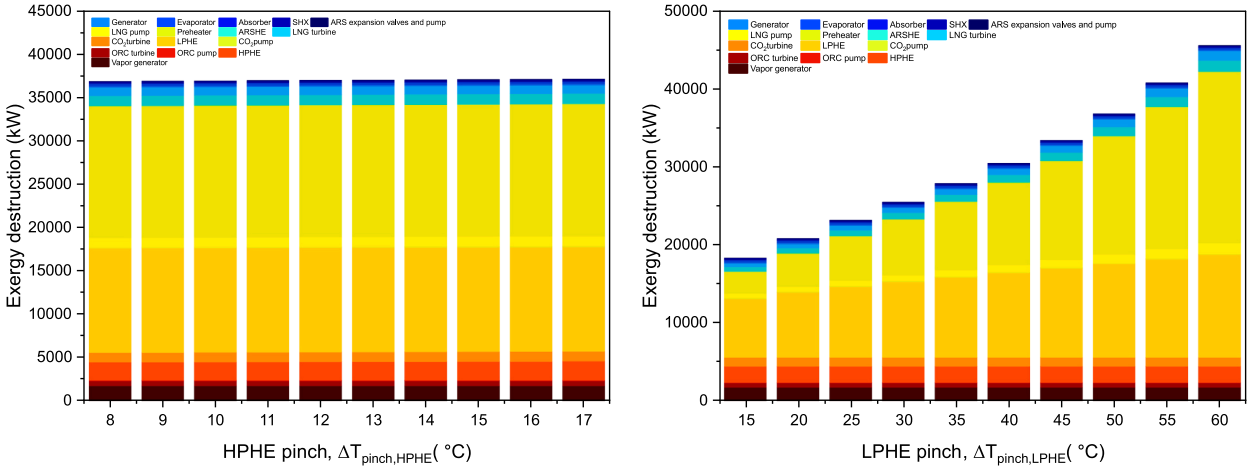

Fig. 23. Effect of exergy destruction with increase in: (a) HPHE pinch temperature. (b) LPHE pinch temperature.

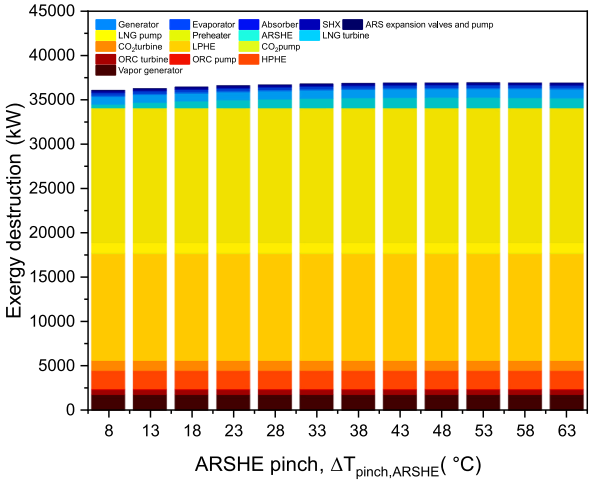

Fig. 24. Effect of exergy destruction rate with increase in ARSHE pinch temperature.

may mitigate this. Among all the components, after EV-1 and EV-2, that has no electrical load, the least cost is observed to be in ARSHE at 0.224 $/h. This can also outline that, the ARSHE should be put through the LNG stream before the preheater. This may incur additional costs, but may reduce the overall costs of the system. In average, the turbines show the highest cost rate, with the TCO_2 turbine being the highest at 150.2 $/h. Moreover, the LNG pump is reported to have a relatively high cost rate, at 11.39 $/h, compared to the rest of the pumps. The average energy cost is 9.121 $/GJ. This can be reduced further by further optimization.

8.5. *Optimization results and performance comparison with similar thermodynamic systems*

The number of hidden layers is crucial in reducing mean squared error (MSE) in an ANN-based objective function [77]. Therefore, to reduce the MSE, a parametric analysis is conducted by varying the number of hidden layers. From the visual interpretation shown in Fig. 25, it was observed that, with a lower number of hidden layers, the objective function may be underfitted, where the model struggles to fit the data. Conversely, a high number of hidden layers can cause overfitting, where the model fits the inherent errors in the dataset too closely [78]. Both these phenomena can result in a high MSE. An optimal point is found when the number of hidden layers were chosen to be 27.

The performance test curve in Fig. 26 illustrates consistency between training and test curves. As shown in Table 17, the MSE of the training and test data is low with relatively minimum error. This suggests that the objective function can accurately predict the non-linear relations between the different functions. Utilizing the generated objective function, multi-objective optimization was performed using Genetic Algorithm (GA). The optimal point from the generated pareto front, shown in Fig. 27, was found using TOPSIS (Technique for Order Preference by Similarity to Ideal Solution) with equal weightage to both output parameters. The pareto front is

Table 16
Capital cost rate of each component of the ACPLU system and total cost.

Capital cost rate	Value ($/h)
$\dot{Z}_{vapor\ generator}$	1.357
$\dot{Z}_{HPHE}$	1.526
$\dot{Z}_{LPHE}$	0.805
$\dot{Z}_{preheater}$	3.263
$\dot{Z}_{turbine,ORC}$	138.9
$\dot{Z}_{turbine,CO_2}$	150.2
$\dot{Z}_{turbine,LNG}$	145.1
$\dot{Z}_{pump,ORC}$	3.126
$\dot{Z}_{pump,CO_2}$	3.934
$\dot{Z}_{pump,LNG}$	11.39
$\dot{Z}_{EV-1}$	0.01
$\dot{Z}_{EV-2}$	0.01
$\dot{Z}_{generator}$	1.14
$\dot{Z}_{ARSHE}$	0.224
$\dot{Z}_{evaporator}$	0.622
$\dot{Z}_{absorber}$	1.057
$\dot{Z}_{SHX}$	1.308
$\dot{Z}_{Total}$	463.8
Average cost per unit power	Value ($/GJ)
c_{ACPLU}	9.121

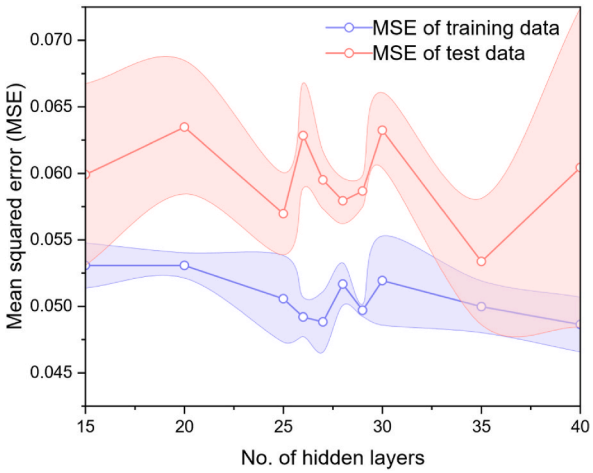

Fig. 25. The variation of mean squared error (MSE) with increasing number of hidden layers. Each point in the figure is the mean value generated from 5 iterations at each hidden layer value, with the area around it being the standard deviation of the points.

consistent with the sensitivity analysis of the ACPLU system, where the net work output would increase the system's overall exergy destruction, resulting in a lower second law efficiency. The different combinations of input variables are shown in Table 18, for (A) Maximum second law efficiency; (B) Optimal; (C) Maximum power. The ARSHE pinch temperature should be kept at the maximum value for maximum performance. The CO_2 condenser pressure is kept at a maximum for maximum second law efficiency, and at minimum for maximum power output. The heat source temperature, however, is kept at a minimum for maximum second law efficiency of 29.82 %. This is evident from the exergy analysis, as a greater heat source temperature would result in more heat being wasted relative to the utilized degree of superheating temperature. But increasing the heat source temperature would results in more net work output from all the cycles; hence the maximum heat source temperature of 450 °C was chosen to generate the maximum net work done of 21.454 MW.

Table 19 provides a general comparison of the net power output, second law efficiency, and COP between previous thermodynamic systems and the ACPLU. It is important to note that the comparison of thermodynamic systems, including CCPs, are not fully comparable due to various factors such as: input temperature, the cycle's upper and lower pressure, cycle component efficiency and working fluid can have a significant impact in the overall performance of the system. That is why, the comparison is limited to combined systems that have at least two common cycles with the ACPLU or has a combined WHR system. With these conditions in

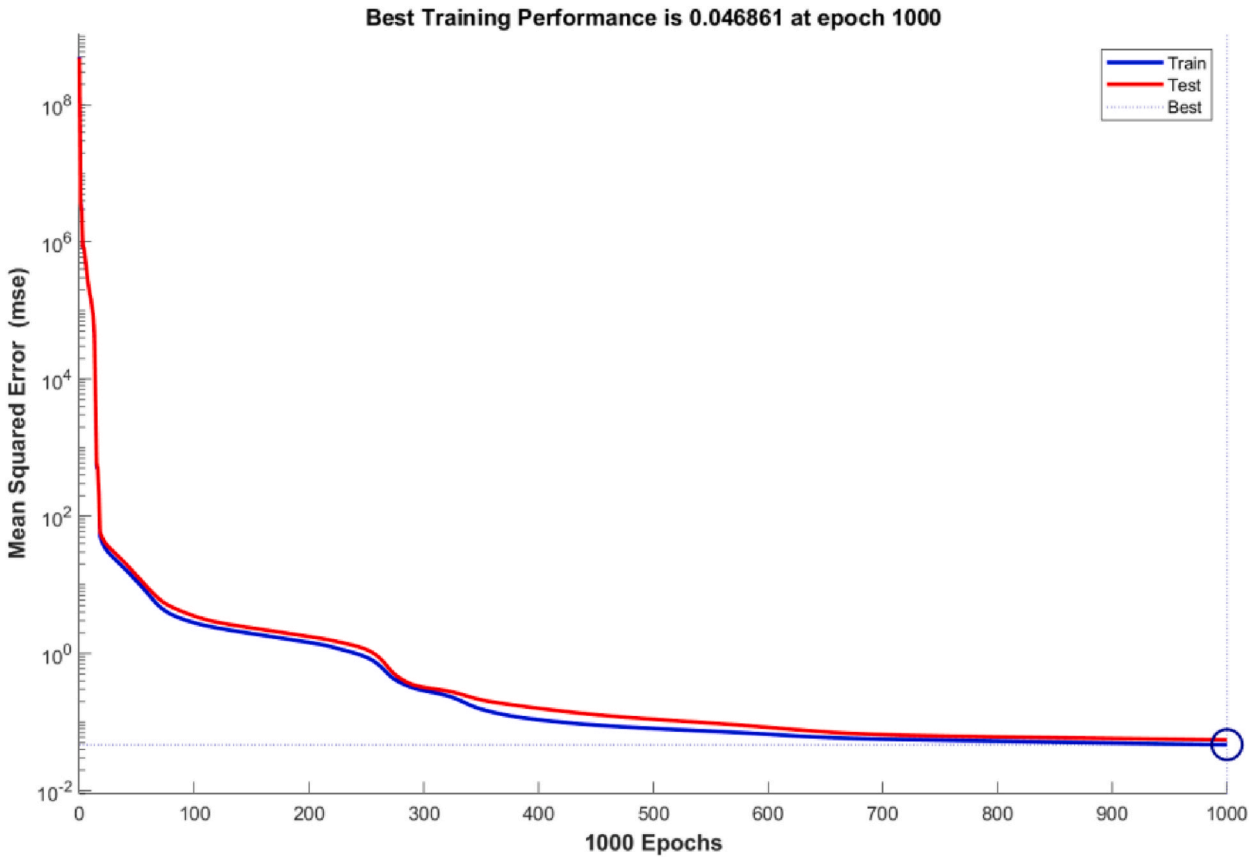

Fig. 26. Performance test analyis of the ANN objective function.

Table 17
The performance of the objective function generated by ANN fitting.

	Observations	MSE	R^2
Training	950	0.0469	1.0000
Test	238	0.0550	1.0000

mind, Table 18 shows that, compared to similar thermodynamic systems, the ACPLU has shown significantly greater net work output and COP without sacrificing second law efficiency. Most of the systems from the literature have shown greater second law efficiency with the expense of relatively very low power output. The only exception is the system proposed by Wang et al. [41], who's performance exceeds the ACPLU in terms of power and second law efficiency, with a relatively small decrease in COP. However, it is worthy to note that, the performance is higher as multiple heat sources have been used, with the highest temperature exceeding 600 °C, while the highest temperature of the ACPLU is recorded to be 300 °C.

9. Conclusion

With the aim of improving existing conventional combined cooling and power (CCP) cycles, an "Advanced Cooling and Power with LNG Utilization (ACPLU)" system is proposed that effectively harnesses waste heat from a moderate temperature heat source. Through the integration of an ORC and ARS, the system demonstrates superior performance compared to previously reported ORC-TCO_2-LNG systems, yielding several key findings.

- By studying different working fluids for the ORC (shown in Table 14), the ACPLU system can achieve the highest second law efficiency of 29.06 % and net work output of 12.27 MW, with cyclopentane as its working fluid. Utilizing LNG cold energy as a heat sink for both the TCO_2 cycle and ARS resulted in this enhanced performance, while also producing re-gasified LNG.
- Increasing heat source temperature has an adverse effect on the ACPLU performance. Hence, this system is ideal for medium-temperature heat source-based waste heat recovery systems.
- A high turbine inlet pressure favours net work and second law efficiency.

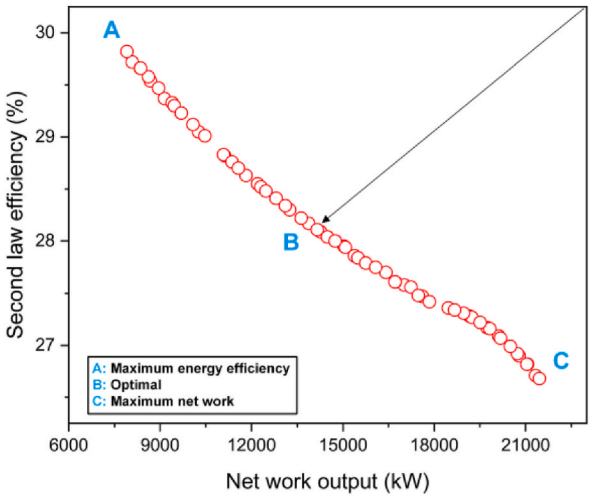

Fig. 27. Pareto front illustrating optimized operating parameters.

Table 18
Combinations of input for: (A) Maximum second law efficiency; (B) Optimal; (C) Maximum power.

Condition		Input			Output	
		Heat source temperature (°C)	CO_2 condenser pressure (bar)	ARSHE pinch (°C)	Second law efficiency	Net work (kW)
A	Maximum second law efficiency	257.6	14	63	29.82	7911
B	Optimal	378.8	14	63	28.11	14159
C	Maximum power	450	6.006	63	26.68	21454

Table 19
Performance comparison between different thermodynamic systems and the ACPLU.

Ref.	Power cycle	Refrigeration cycle	Working fluids	Performance (From literature)			Performance (ACPLU)		
				Net work (MW)	2nd law efficiency (%)	COP	Net work (MW)	2nd law efficiency (%)	COP
Sadreddini et al. [5]	Cascaded ORC-TCO_2 + LNG open cycle	–	Pentane, CO_2, LNG, water	8.12	13.1	–	14.16	28.1	0.7403
Dadpour et al. [15]	Cascaded ORC-high pressure TCO_2-low pressure CO_2 + LNG open cycle	–	Pentane, CO_2, LNG	6.41	15.2	–			
Liang et al. [4]	Dual loop CO_2 Brayton cycle + ORC	–	R1233zd(E), CO_2	0.291	48.4	–			
Sadreddini et al. [10]	Compressed air energy storage + ORC	Ejector refrigeration	Water, toluene, R123	0.034	68.0	0.09			
Mardan Dezfouli et al. [22]	Cascaded ORC-TCO_2 + LNG open cycle	–	Pentane, CO_2, LNG	1.446	65.7	–			
Wang et al. [41]	Cascaded SCO_2 Brayton-ORC	Absorption refrigeration	CO_2, butane, water, NH_3–H_2O	40.65	48.57	0.57			
Y. Li et al. [44]	Rankine cycle + LNG open cycle	Absorption refrigeration	Water, LNG, NH_3–H_2O	0.505	35.14	0.72			
Higa et al. [45]	Kalina cycle	Absorption refrigeration	NH_3–H_2O	0.493	46.8	0.38			

- The components of the LNG stream (i.e., LPHE, preheater) reported the highest amount of exergy destruction. The most important parameters for exergy destruction are the heat source temperature, CO_2 condenser pressure, and LPHE pinch.
- A higher generator temperature improves COP. An evaporator temperature of 0 °C also favours both COP and second law efficiency.

- From the optimization results using ANN and GA, it is observed that a low heat source temperature favours high second law efficiency, while a high one favours net power output. However, the inverse is observed for CO_2 condenser pressure. An optimal combination of heat source temperature: 378.8 °C; CO_2 condenser pressure: 14 bar; ARSHE pinch temperature: 63 °C, is observed to give a higher performance than the initial conditions used in the study.
- The preheater is shown to have the highest cost rate among heat exchangers, at 3.263 $/h. The highest cost rate is observed in the turbines (~150 $/h), and a relatively high cost rate is also reported by the LNG pump (11.39 $/h).

The ACPLU was able to address the need for effective utilization of energy from moderate-temperature exhaust heat when an LNG open cycle is used as the heat sink for the transcritical CO_2 (TCO_2) cycle, without suffering from overwhelming low efficiency.

Recommendations for future study

The innovation of the Advanced Cooling and Power with LNG Utilization (ACPLU) lies in its ability to simultaneously generate cooling and power by utilizing moderate temperature heat, specifically through the re-gasifying Liquefied Natural Gas (LNG). This integrated approach not only maximizes the utility of available thermal energy but also minimizes energy waste. We have primarily relied on theoretical models, thermodynamic calculations, and optimization techniques in order to explore the performance of the ACPLU system in this study. Keeping the importance of practical feasibility considerations, future research directions could include empirical studies to evaluate the system performance in real-world scenarios, considering factors such as site-specific conditions, regulatory requirements, and environmental impacts which would provide valuable insights into the actual spatial requirements. The ACPLU system is well-suited for pharmaceutical manufacturing plants. The cooling effect can be used for cold storage of medicine, as well as blood samples, drugs etc. The re-gasified LNG can also be used for boiler heating, as well as in burners. The results of this analysis will provide concrete data to support the hypothesis that this system is a suitable and advantageous solution for pharmaceutical plants. Some recommendations are.

- Considering the high exergy destruction in the LNG stream, a comprehensive study of the exergy destruction of an LNG open cycle when implemented as a heat sink is recommended. In addition to physical exergy, future studies should consider chemical exergy, and focus on reducing the relatively high exergy destruction from the LNG cycle components.
- The cost rate among heat exchangers suggests that, while the preheater improves the overall performance of the WHR system, it should be placed in a way where the heat transfer in the preheater can decrease.
- CO_2 capturing system: By leveraging the cold energy from LNG during its regasification process, a CO_2 capture process can be implemented when cooling down the factory exhaust gases. Lower energy requirements and increased efficiency can result in cost savings for industries implementing this innovation but there are challenges to address, such as engineering considerations for integrating the systems, optimizing the process for varying exhaust gas compositions, and ensuring compatibility with existing industrial infrastructure.
- Cooling of parallel thermodynamic systems: The integration of a low-temperature heat sink such as LNG, can allow the advent of more complex systems as it can act as a heat sink for several closed cycles. This concept presents an intriguing avenue for enhancing energy efficiency and reducing environmental impact across various industrial and commercial applications, including refrigeration, air conditioning, food processing, and industrial cooling. Continued research, development, and implementation of this technology can contribute to a more sustainable and resilient energy future.

Data availability statement

The authors have initially validated the code with a reference model. Subsequently, a dataset has been generated to train a regression model for further works in this paper. If this dataset proves beneficial for future endeavours in this sector, the authors will make it available on request.

Ethics statement

The study did not necessitate review and/or approval by an ethics committee, as it exclusively involves a software-based simulation of a combined cooling and power system. The authors systematically developed a model, validated it against a reference model, and subsequently developed their proposed system. Given the non-invasive nature of the study and the absence of involvement with human subjects, the need for informed consent was not required as well.

CRediT authorship contribution statement

Tajwar A. Baigh: Writing – original draft, Visualization, Validation, Software, Methodology, Investigation, Formal analysis, Data curation, Conceptualization. **Mostofa J. Saif:** Writing – original draft, Visualization, Validation, Software, Methodology, Investigation, Formal analysis, Data curation, Conceptualization. **Ashraf Mustakim:** Writing – original draft, Visualization, Validation, Software, Methodology, Investigation, Formal analysis, Data curation. **Fairooz Nanzeeba:** Writing – original draft, Visualization, Software, Investigation, Formal analysis, Data curation. **Yasin Khan:** Writing – review & editing, Validation, Supervision, Project administration, Conceptualization. **M. Monjurul Ehsan:** Writing – review & editing, Supervision, Project administration,

Conceptualization.

Declaration of competing interest

The authors declare that they have no known competing financial interests or personal relationships that could have appeared to influence the work reported in this paper.

References

[1] Y. Ammar, S. Joyce, R. Norman, Y. Wang, A.P. Roskilly, Low grade thermal energy sources and uses from the process industry in the UK, Appl. Energy 89 (2012) 3–20, https://doi.org/10.1016/j.apenergy.2011.06.003.

[2] W. Gao, Z. Wu, Z. Tian, Y. Zhang, Experimental investigation on an R290-based organic Rankine cycle utilizing cold energy of liquid nitrogen, Appl. Therm. Eng. 202 (2022), https://doi.org/10.1016/j.applthermaleng.2021.117757.

[3] H. Wang, X. Shi, D. Che, Thermodynamic optimization of the operating parameters for a combined power cycle utilizing low-temperature waste heat and LNG cold energy, Appl. Therm. Eng. 59 (2013) 490–497, https://doi.org/10.1016/j.applthermaleng.2013.05.048.

[4] Y. Liang, X. Bian, W. Qian, M. Pan, Z. Ban, Z. Yu, Theoretical analysis of a regenerative supercritical carbon dioxide Brayton cycle/organic Rankine cycle dual loop for waste heat recovery of a diesel/natural gas dual-fuel engine, Energy Convers. Manag. 197 (2019), https://doi.org/10.1016/j.enconman.2019.111845.

[5] A. Sadreddini, M.A. Ashjari, M. Fani, A. Mohammadi, Thermodynamic analysis of a new cascade ORC and transcritical CO2 cycle to recover energy from medium temperature heat source and liquefied natural gas, Energy Convers. Manag. 167 (2018) 9–20, https://doi.org/10.1016/j.enconman.2018.04.093.

[6] F. Fatigati, D. Vittorini, M. di Bartolomeo, R. Cipollone, Experimental characterization of a small-scale solar Organic Rankine Cycle (ORC) based unit for domestic microcogeneration, Energy Convers. Manag. 258 (2022), https://doi.org/10.1016/j.enconman.2022.115493.

[7] L. Wang, X. Huang, M. Babaei, Z. Liu, X. Yang, J. Yan, Full-scale utilization of geothermal energy: a high-efficiency CO2 hybrid cogeneration system with low-temperature waste heat, J. Clean. Prod. 403 (2023) 136866, https://doi.org/10.1016/j.jclepro.2023.136866.

[8] P. Ziółkowski, T. Kowalczyk, S. Kornet, J. Badur, On low-grade waste heat utilization from a supercritical steam power plant using an ORC-bottoming cycle coupled with two sources of heat, Energy Convers. Manag. 146 (2017) 158–173, https://doi.org/10.1016/j.enconman.2017.05.028.

[9] O. Dumont, R. Dickes, M. de Rosa, R. Douglas, V. Lemort, Technical and economic optimization of subcritical, wet expansion and transcritical Organic Rankine Cycle (ORC) systems coupled with a biogas power plant, Energy Convers. Manag. 157 (2018) 294–306, https://doi.org/10.1016/j.enconman.2017.12.022.

[10] A. Sadreddini, M. Fani, M. Ashjari Aghdam, A. Mohammadi, Exergy analysis and optimization of a CCHP system composed of compressed air energy storage system and ORC cycle, Energy Convers. Manag. 157 (2018) 111–122, https://doi.org/10.1016/j.enconman.2017.11.055.

[11] M. Deymi-Dashtebayaz, M. Norani, Sustainability assessment and emergy analysis of employing the CCHP system under two different scenarios in a data center, Renew. Sustain. Energy Rev. 150 (2021) 111511, https://doi.org/10.1016/j.rser.2021.111511.

[12] H. Yagli, A. Koc, C. Karakus, Y. Koc, Comparison of toluene and cyclohexane as a working fluid of an organic Rankine cycle used for reheat furnace waste heat recovery, Int. J. Exergy 19 (2016) 420, https://doi.org/10.1504/IJEX.2016.075677.

[13] I. Andrić, A. Pina, P. Ferrão, J. Fournier, B. Lacarrière, O. le Corre, Assessing the feasibility of using the heat demand-outdoor temperature function for a long-term district heat demand forecast, Energy Proc. 116 (2017) 460–469, https://doi.org/10.1016/j.egypro.2017.05.093.

[14] M.M. Ehsan, Z. Guan, A.Y. Klimenko, A comprehensive review on heat transfer and pressure drop characteristics and correlations with supercritical CO 2 under heating and cooling applications, Renew. Sustain. Energy Rev. 92 (2018) 658–675, https://doi.org/10.1016/j.rser.2018.04.106.

[15] D. Dadpour, M. Deymi-Dashtebayaz, M. Delpisheh, S.A. Naghibi Fard, A <scp>3E</scp> analysis of a multi-power generation system employing <scp> CO $_2$ </scp> , <scp>LNG</scp> , and Organic Rankine cycles, Environ. Prog. Sustain. Energy 43 (2024), https://doi.org/10.1002/ep.14349.

[16] H. Liu, L. You, Characteristics and Applications of the Cold Heat Exergy of Lique®ed Natural Gas, n.d.

[17] W.J. Rao, L.J. Zhao, C. Liu, M.G. Zhang, A combined cycle utilizing LNG and low-temperature solar energy, Appl. Therm. Eng. 60 (2013) 51–60, https://doi.org/10.1016/j.applthermaleng.2013.06.043.

[18] M. Romero Gómez, R. Ferreiro Garcia, J. Romero Gómez, J. Carbia Carril, Review of thermal cycles exploiting the exergy of liquefied natural gas in the regasification process, Renew. Sustain. Energy Rev. 38 (2014) 781–795, https://doi.org/10.1016/j.rser.2014.07.029.

[19] J. Wang, J. Wang, Y. Dai, P. Zhao, Thermodynamic analysis and optimization of a transcritical CO2 geothermal power generation system based on the cold energy utilization of LNG, Appl. Therm. Eng. 70 (2014) 531–540, https://doi.org/10.1016/j.applthermaleng.2014.05.084.

[20] Y. Song, J. Wang, Y. Dai, E. Zhou, Thermodynamic analysis of a transcritical CO2 power cycle driven by solar energy with liquified natural gas as its heat sink, Appl. Energy 92 (2012) 194–203, https://doi.org/10.1016/j.apenergy.2011.10.021.

[21] W. Lin, M. Huang, H. He, A. Gu, A transcritical CO2 Rankine cycle with LNG cold energy utilization and liquefaction of CO2 in gas turbine exhaust, Journal of Energy Resources Technology, Transactions of the ASME 131 (2009) 422011–422015, https://doi.org/10.1115/1.4000176.

[22] A.H. Mardan Dezfouli, N. Niroozadeh, A. Jahangiri, Energy, exergy, and exergoeconomic analysis and multi-objective optimization of a novel geothermal driven power generation system of combined transcritical CO2 and C5H12 ORCs coupled with LNG stream injection, Energy 262 (2023) 125316, https://doi.org/10.1016/j.energy.2022.125316.

[23] M.W. Faruque, M.R. Uddin, S. Salehin, M.M. Ehsan, A comprehensive thermodynamic assessment of cascade refrigeration system utilizing low GWP hydrocarbon refrigerants, International Journal of Thermofluids 15 (2022) 100177, https://doi.org/10.1016/j.ijft.2022.100177.

[24] M. Walid Faruque, M. Hafiz Nabil, M. Raihan Uddin, M. Monjurul Ehsan, S. Salehin, Thermodynamic assessment of a triple cascade refrigeration system utilizing hydrocarbon refrigerants for ultra-low temperature applications, Energy Convers. Manag. X 14 (2022) 100207, https://doi.org/10.1016/j.ecmx.2022.100207.

[25] M. Walid Faruque, Y. Khan, M. Hafiz Nabil, M. Monjurul Ehsan, A. Karim, Thermal performance evaluation of a novel ejector-injection cascade refrigeration system, Therm. Sci. Eng. Prog. 39 (2023) 101745, https://doi.org/10.1016/j.tsep.2023.101745.

[26] M. Higa, E.Y. Yamamoto, J.C.D. de Oliveira, W.A.S. Conceição, Evaluation of the integration of an ammonia-water power cycle in an absorption refrigeration system of an industrial plant, Energy Convers. Manag. 178 (2018) 265–276, https://doi.org/10.1016/j.enconman.2018.10.041.

[27] D.A. Selvaraj, K. Victor, Design and performance of solar PV integrated domestic vapor absorption refrigeration system, Int. J. Photoenergy 2021 (2021) 1–10, https://doi.org/10.1155/2021/6655113.

[28] A. Keçeciler, H.İ. Acar, A. Doğan, Thermodynamic analysis of the absorption refrigeration system with geothermal energy: an experimental study, Energy Convers. Manag. 41 (2000) 37–48, https://doi.org/10.1016/S0196-8904(99)00091-6.

[29] M. Mbikan, T. Al-Shemmeri, Computational model of a biomass driven absorption refrigeration system, Energies 10 (2017), https://doi.org/10.3390/en10020234.

[30] Z.Y. Xu, R.Z. Wang, Absorption refrigeration cycles: categorized based on the cycle construction, Int. J. Refrig. 62 (2016) 114–136, https://doi.org/10.1016/j.ijrefrig.2015.10.007.

[31] R. Nikbakhti, X. Wang, A.K. Hussein, A. Iranmanesh, Absorption cooling systems – review of various techniques for energy performance enhancement, Alex. Eng. J. 59 (2020) 707–738, https://doi.org/10.1016/j.aej.2020.01.036.

[32] M.W. Faruque, Y. Khan, M.H. Nabil, M.M. Ehsan, Parametric analysis and optimization of a novel cascade compression-absorption refrigeration system integrated with a flash tank and a reheater, Results in Engineering 17 (2023) 101008, https://doi.org/10.1016/j.rineng.2023.101008.

[33] M.H. Nabil, Y. Khan, M.W. Faruque, M.M. Ehsan, Thermo-economic assessment of advanced triple cascade refrigeration system incorporating a flash tank and suction line heat exchanger, Energy Convers. Manag. 295 (2023) 117630, https://doi.org/10.1016/j.enconman.2023.117630.

[34] R. Maryami, A.A. Dehghan, An exergy based comparative study between LiBr/water absorption refrigeration systems from half effect to triple effect, Appl. Therm. Eng. 124 (2017) 103–123, https://doi.org/10.1016/j.applthermaleng.2017.05.174.

[35] W. Salmi, J. Vanttola, M. Elg, M. Kuosa, R. Lahdelma, Using waste heat of ship as energy source for an absorption refrigeration system, Appl. Therm. Eng. 115 (2017) 501–516, https://doi.org/10.1016/j.applthermaleng.2016.12.131.

[36] P. Rodgers, A. Mortazavi, V. Eveloy, S. Al-Hashimi, Y. Hwang, R. Radermacher, Enhancement of LNG plant propane cycle through waste heat powered absorption cooling, Appl. Therm. Eng. 48 (2012) 41–53, https://doi.org/10.1016/j.applthermaleng.2012.04.031.

[37] S. Zhou, G. He, Y. Li, X. Liang, Q. Pang, D. Cai, Comprehensive experimental evaluation of an exhaust-heat-driven absorption refrigeration cycle system using NH3-NaSCN as working pair, Int. J. Refrig. 126 (2021) 168–180, https://doi.org/10.1016/j.ijrefrig.2021.01.013.

[38] H. Nami, A. Arabkoohsar, Improving the power share of waste-driven CHP plants via parallelization with a small-scale Rankine cycle, a thermodynamic analysis, Energy 171 (2019) 27–36, https://doi.org/10.1016/j.energy.2018.12.168.

[39] X. Wang, C. Yang, M. Huang, X. Ma, Off-design performances of gas turbine-based CCHP combined with solar and compressed air energy storage with organic Rankine cycle, Energy Convers. Manag. 156 (2018) 626–638, https://doi.org/10.1016/j.enconman.2017.11.082.

[40] S.S. Bishal, D.F. Faysal, M.M. Ehsan, S. Salehin, Performance evaluation of an integrated cooling and power system combining supercritical CO2, gas turbine, absorption refrigeration, and organic rankine cycles for waste energy recuperating system, Results in Engineering 17 (2023) 100943, https://doi.org/10.1016/j.rineng.2023.100943.

[41] S. Wang, C. Liu, J. Li, Z. Sun, X. Chen, X. Wang, Exergoeconomic analysis of a novel trigeneration system containing supercritical CO2 Brayton cycle, organic Rankine cycle and absorption refrigeration cycle for gas turbine waste heat recovery, Energy Convers. Manag. 221 (2020) 113064, https://doi.org/10.1016/j.enconman.2020.113064.

[42] S. Yang, C. Deng, Z. Liu, Optimal design and analysis of a cascade LiBr/H2O absorption refrigeration/transcritical CO2 process for low-grade waste heat recovery, Energy Convers. Manag. 192 (2019) 232–242, https://doi.org/10.1016/j.enconman.2019.04.045.

[43] X. Liu, X. Yang, M. Yu, W. Zhang, Y. Wang, P. Cui, Z. Zhu, Y. Ma, J. Gao, Energy, exergy, economic and environmental (4E) analysis of an integrated process combining CO2 capture and storage, an organic Rankine cycle and an absorption refrigeration cycle, Energy Convers. Manag. 210 (2020) 112738, https://doi.org/10.1016/j.enconman.2020.112738.

[44] Y. Li, Y. Liu, G. Zhang, Y. Yang, Thermodynamic analysis of a novel combined cooling and power system utilizing liquefied natural gas (LNG) cryogenic energy and low-temperature waste heat, Energy 199 (2020) 117479, https://doi.org/10.1016/j.energy.2020.117479.

[45] M. Higa, E.Y. Yamamoto, J.C.D. de Oliveira, W.A.S. Conceição, Evaluation of the integration of an ammonia-water power cycle in an absorption refrigeration system of an industrial plant, Energy Convers. Manag. 178 (2018) 265–276, https://doi.org/10.1016/j.enconman.2018.10.041.

[46] H. Li, W. Su, L. Cao, F. Chang, W. Xia, Y. Dai, Preliminary conceptual design and thermodynamic comparative study on vapor absorption refrigeration cycles integrated with a supercritical CO2 power cycle, Energy Convers. Manag. 161 (2018) 162–171, https://doi.org/10.1016/j.enconman.2018.01.065.

[47] J. Sun, L. Fu, S. Zhang, A review of working fluids of absorption cycles, Renew. Sustain. Energy Rev. 16 (2012) 1899–1906, https://doi.org/10.1016/j.rser.2012.01.011.

[48] M. Deymi-Dashtebayaz, S. Maddah, M. Goodarzi, O. Maddah, Investigation of the effect of using various HFC refrigerants in geothermal heat pump with residential heating applications, J. Therm. Anal. Calorim. 141 (2020) 361–372, https://doi.org/10.1007/s10973-020-09539-5.

[49] I. Horuz, A comparison between ammonia-water and water-lithium bromide solutions in vapor absorption refrigeration systems, Int. Commun. Heat Mass Tran. 25 (1998) 711–721, https://doi.org/10.1016/S0735-1933(98)00058-X.

[50] S.A. kumar, R. Ragavendran, Design and fabrication of solar powered lithium bromide vapour absorption refrigeration system, IOSR J. Mech. Civ. Eng. 13 (2016) 57–62, https://doi.org/10.9790/1684-1304025762.

[51] N.A. Ghyadh, Overview of working pair used in absorption refrigeration technologies, Int. J. Res. Appl. Sci. Eng. Technol. 6 (2018) 662–678, https://doi.org/10.22214/ijraset.2018.7114.

[52] B. Modi, A. Mudgal, B. Patel, Energy and exergy investigation of small capacity single effect lithium bromide absorption refrigeration system, Energy Proc. 109 (2017) 203–210, https://doi.org/10.1016/j.egypro.2017.03.040.

[53] M.O. McLinden, E.W. Lemmon, R.T. Jacobsen, Thermodynamic properties for the alternative refrigerants, Int. J. Refrig. 21 (1998) 322–338, https://doi.org/10.1016/S0140-7007(97)00081-9.

[54] J. Deng, R.Z. Wang, G.Y. Han, A review of thermally activated cooling technologies for combined cooling, heating and power systems, Prog. Energy Combust. Sci. 37 (2011) 172–203, https://doi.org/10.1016/j.pecs.2010.05.003.

[55] Y. Khan, M.W. Faruque, M.H. Nabil, M.M. Ehsan, Ejector and vapor injection enhanced novel compression-absorption cascade refrigeration systems: a thermodynamic parametric and refrigerant analysis, Energy Convers. Manag. 289 (2023), https://doi.org/10.1016/j.enconman.2023.117190.

[56] B. Modi, A. Mudgal, B. Patel, Energy and exergy investigation of small capacity single effect lithium bromide absorption refrigeration system, in: Energy Procedia, Elsevier Ltd, 2017, pp. 203–210, https://doi.org/10.1016/j.egypro.2017.03.040.

[57] H. Ghaebi, T. Parikhani, H. Rostamzadeh, B. Farhang, Thermodynamic and thermoeconomic analysis and optimization of a novel combined cooling and power (CCP) cycle by integrating of ejector refrigeration and Kalina cycles, Energy 139 (2017) 262–276, https://doi.org/10.1016/j.energy.2017.07.154.

[58] A. Yu, W. Su, X. Lin, N. Zhou, L. Zhao, Thermodynamic analysis on the combination of supercritical carbon dioxide power cycle and transcritical carbon dioxide refrigeration cycle for the waste heat recovery of shipboard, Energy Convers. Manag. 221 (2020), https://doi.org/10.1016/j.enconman.2020.113214.

[59] M.H. Ahmadi, A. Mohammadi, F. Pourfayaz, M. Mehrpooya, M. Bidi, A. Valero, S. Uson, Thermodynamic analysis and optimization of a waste heat recovery system for proton exchange membrane fuel cell using transcritical carbon dioxide cycle and cold energy of liquefied natural gas, J. Nat. Gas Sci. Eng. 34 (2016) 428–438, https://doi.org/10.1016/j.jngse.2016.07.014.

[60] A.V. Finkelstein, S.O. Garbuzynskiy, B.S. Melnik, How can ice emerge at 0 °C? Biomolecules 12 (2022) 981, https://doi.org/10.3390/biom12070981.

[61] P.J. Williams, The freezing of soils: ice in a porous medium and its environmental significance, in: Ice Physics and the Natural Environment, Springer Berlin Heidelberg, Berlin, Heidelberg, 1999, pp. 219–239, https://doi.org/10.1007/978-3-642-60030-2_13.

[62] A.K. Jain, Jianchang Mao, K.M. Mohiuddin, Artificial neural networks: a tutorial, Computer (Long Beach Calif) 29 (1996) 31–44, https://doi.org/10.1109/2.485891.

[63] A. Krogh, What are artificial neural networks? Nat. Biotechnol. 26 (2008) 195–197, https://doi.org/10.1038/nbt1386.

[64] Y. Feng, K. Xu, Q. Zhang, T.-C. Hung, Z. He, H. Xi, N. Rasheed, Experimental investigation and machine learning optimization of a small-scale organic Rankine cycle, Appl. Therm. Eng. 224 (2023) 120120, https://doi.org/10.1016/j.applthermaleng.2023.120120.

[65] S. Kowsari, M. Deymi-Dashtebayaz, K. Karbasi, H. Sheikhani, Optimal working conditions of various city gate stations for power and hydrogen production based on energy and eco-exergy analysis, Int. J. Hydrogen Energy 45 (2020) 22513–22533, https://doi.org/10.1016/j.ijhydene.2020.05.110.

[66] V. Srinivas, K. Ramanjaneyulu, An integrated approach for optimum design of bridge decks using genetic algorithms and artificial neural networks, Adv. Eng. Software 38 (2007) 475–487, https://doi.org/10.1016/j.advengsoft.2006.09.016.

[67] E. Lemmon, M. Huber, M. McLinden, NIST Standard Reference Database 23: Reference Fluid Thermodynamic and Transport Properties-REFPROP, 2007, Version 8.0.

[68] B.A. Younglove, M.O. McLinden, An international standard equation of state for the thermodynamic properties of refrigerant 123 (2,2-Dichloro-1,1,1-Trifluoroethane), J. Phys. Chem. Ref. Data 23 (1994) 731–779, https://doi.org/10.1063/1.555950.

[69] E.W. Lemmon, R. Span, Short fundamental equations of state for 20 industrial fluids, J. Chem. Eng. Data 51 (2006) 785–850, https://doi.org/10.1021/je050186n.

[70] R. Span, W. Wagner, A new equation of state for carbon dioxide covering the fluid region from the triple-point temperature to 1100 K at pressures up to 800 MPa, J. Phys. Chem. Ref. Data 25 (1996) 1509–1596, https://doi.org/10.1063/1.555991.

[71] R. Akasaka, Y. Zhou, E.W. Lemmon, A fundamental equation of state for 1,1,1,3,3-pentafluoropropane (R-245fa), J. Phys. Chem. Ref. Data 44 (2015), https://doi.org/10.1063/1.4913493.

[72] H. Gedanitz, M.J. Davila, E.W. Lemmon, Speed of sound measurements and a fundamental equation of state for cyclopentane, J. Chem. Eng. Data 60 (2015) 1331–1337, https://doi.org/10.1021/je5010164.

[73] Y. Zhou, J. Wu, E.W. Lemmon, Thermodynamic Properties of *o* -Xylene, *m* -Xylene, *p* -Xylene, and Ethylbenzene, J. Phys. Chem. Ref. Data 41 (2012) 23103, https://doi.org/10.1063/1.3703506, 023103–26.
[74] J. Smukala, R. Span, W. Wagner, New equation of state for ethylene covering the fluid region for temperatures from the melting line to 450 K at pressures up to 300 MPa, J. Phys. Chem. Ref. Data 29 (2000) 1053–1121, https://doi.org/10.1063/1.1329318.
[75] S.S. Christopher, R. Santosh, M. Ponrajan Vikram, R. Prabakaran, A.K. Thakur, H. Xu, Optimization of a solar water heating system for vapor absorption refrigeration system, Environ. Prog. Sustain. Energy 40 (2021), https://doi.org/10.1002/ep.13489.
[76] Y. Gao, G. He, P. Chen, X. Zhao, D. Cai, Energy and exergy analysis of an air-cooled waste heat-driven absorption refrigeration cycle using R290/oil as working fluid, Energy 173 (2019) 820–832, https://doi.org/10.1016/j.energy.2019.02.117.
[77] K.G. Sheela, S.N. Deepa, Review on methods to fix number of hidden neurons in neural networks, Math. Probl Eng. 2013 (2013) 1–11, https://doi.org/10.1155/2013/425740.
[78] F. Fleuret, The Little Book of Deep Learning, 2023.